Fall 2014

Profile of the unfolded protein response in C. elegans depleted of the translational chaperone, NAC.

Caylin S. Murray
James Madison University

Profile of the Unfolded Protein Response in *C. elegans* depleted of the translational chaperone, NAC.

Caylin Murray

A thesis submitted to the Graduate Faculty of

JAMES MADISON UNIVERSITY

In

Partial Fulfillment of the Requirements

for the degree of

Master of Science

Department of Biology

December 2014

TABLE OF CONTENTS

List of Figures

1. ABSTRACT

The function of a protein is a direct consequence of its final structure, which is achieved by protein-folding processes that generate a tertiary state through the juxtaposition of locally formed secondary structures. Because all cells need functional proteins to survive, each contains robust and redundant mechanisms that regulate the folding of newly forming proteins, and the refolding of misfolded proteins that are often generated during stress. Essential to these mechanisms, chaperones are proteins that aid in protein folding of nascent and misfolding protein without being incorporated in the final structure. One chaperone complex, the nascent polypeptide-associated complex (NAC), aids in the folding and translocation of nascent peptide chains during translation. Reflecting its importance to protein folding and therefore survival, complete removal of the NAC is embryonic lethal in a number of metazoans, including *Caenorhabditis elegans*, while depletion is enough to stimulate up-regulation of *hsp-4*, an unfolded protein response (UPR) marker that mitigates misfolded protein stress in the ER. To discern the relationship between the NAC and the UPR in the context of misfolded protein stress management, I depleted the NAC in *C. elegans* embryos deficient for specific elements of the UPR and determined subsequent effects on stress-induced phenotypes. Depletion of either *C. elegans* NAC subunit (ICD-1 or ICD-2) in select UPR knock-out mutants (IRE1, XBP-1, PERK and ATF6) resulted in changes in apoptosis, autophagy, morphology, and embryonic development that provided insights into the contributions of different UPR elements to these phenotypes. Through these studies, I determined IRE1 plays the most salient role in the UPR initiated upon depletion of the NAC, being directly involved in both the promotion of apoptosis and the

maintenance of embryonic development during ER-specific misfolded protein stress. PERK/PEK-1 and ATF6 also contribute to the UPR in NAC-depleted embryos, but to a lesser extent. Overall, these studies provide evidence of a direct relationship between two essential stress-management systems responsible for the maintenance of protein homeostasis in all cells.

2. INTRODUCTION

2.1 PROTEIN FOLDING AND MOLECULAR CHAPERONES

The vast scope of organismal diversity and success is a direct result of the evolution of distinct proteins. The study of proteins, which are highly conserved and regulated polymers of amino acids, is paramount because a cell's protein profile ultimately determines the cellular phenotype. The collection of proteins expressed defines the proteome of the organism and is itself defined by the allelic make-up of the cell. Proteins are of vital importance to cell function and the diversity of their functions is reflected in their vast structural diversity. Protein function can be classified as follows: regulatory proteins that control gene activity, transport proteins that facilitate the movement of molecules across membranes, enzymes that catalyze chemical reactions, and structural and scaffolding proteins that determine cell shape and are responsible for transport of resources intrinsically (Lodish et al, 2007). Just as the role of a cell is defined by its protein make-up, the function of a protein is dependent on its three dimensional conformation. Highly conserved amino acid motifs and domains define these conformations, and are the foundation to our understanding of protein function as they are useful to predict the function of novel proteins. Due to the complexities of three dimensional protein-folding and the vital importance of protein function to cell viability, the cell has evolved robust and redundant mechanisms for regulation of protein folding

The blueprint of a protein's structure resides in the sequence of amino acids that constitute the polypeptide chain. Polypeptide chains are assembled via tRNAs bringing collections of amino acids into linear arrays as directed by the codons coded for by

cognate mRNAs passing through the ribosomal complex. Folding begins as the amino acid chain emerges from the ribosome and forms secondary structures. Secondary structures, including α-helical chains and β-pleated sheets, form from repetitive stretches of amino acids held together by hydrogen bonds. Due to their energetic stability, secondary structures represent the majority of the internal support for the protein. The final conformation, or tertiary structure, of the polypeptide is then determined by hydrophobic interactions between hydrogen bonds, peptide bonds, and non-polar side chains directed by secondary structure content (Lodish et al, 2007). These interactions hinder protein fluidity and secure the structure of the protein. While the relationship between side groups and secondary structures is enough to initiate protein folding, certain transitional interactions may generate energetically favorable but poorly functioning intermediates that prevent the protein from reaching proper conformation within a biologically relevant time frame (Vabulas, Raychaudhuri, Hayer-Hartl, & Hartl, 2010). These stable intermediates can be harmful and even toxic to the cell as they are energetically very stable, but result in poorly functioning or nonfunctional proteins that are difficult to degrade.

Complexities in folding increase with amino acid length. Protein folding is the most efficient and precise once 50 to 300 amino acids have emerged from the ribosome. Since translation can be protracted and complex, long amino acid chains can be left exposed to cellular conditions in partially folded states during translation. As this exposure time increases with the complexity and size of the proteins so does the propensity of large proteins to fold improperly. These partially folded intermediates can become problematic in high concentrations, as inappropriate interaction between the

intermediates can result in insoluble aggregates (Vabulas et al., 2010). Early in this process, small amorphous aggregates are formed. These aggregates can develop into large amorphous structures that hinder the proper formation of other proteins in the area. At high concentration, misfolded proteins can associate with each other to form low energy fibrous strands. The fibrils, called amyloid fibers, are difficult for the cell to resolve or degrade. The fibrils develop when hydrophobic regions of proteins are exposed to each other during misfolding. Due to the crowded nature of the cell, misfolded proteins align into the fibers to shield their hydrophobic regions from the aqueous environment, resulting in an aggregation that is difficult to separate or degrade (Vabulas et al., 2010). Such a buildup of amyloid fibrils has been linked with neurodegenerative disease, systemic amyloidosis, and other disease because their accumulation is thought to lead to the death of the cell. While pathologies vary greatly, the accumulation and mismanagement of improperly or completely unfolded proteins are salient in diseases of otherwise independent etiologies as they are a common feature to all. To prevent such occurrences, proteins often fold in ribosome-rich polysome modules centered on important domains thus protecting the domains and ensuring that proper folding occurs (Brandt et al., 2009; Dobson, 2003). Regardless of specific context, however, folding and/or refolding of proteins into proper functional states is a dynamic process that routinely requires a class of proteins called chaperones.

Chaperones are proteins that selectively bind non-native proteins and aid in folding or refolding by forming a stable complex with the protein without being incorporated in its final structure. Chaperones perform several important roles; they: 1) prevent misfolding and aggregation of nascent protein during translation, 2) prevent

inappropriate interaction with unnecessary cellular components, 3) aid in the assembly of large proteins and those with quaternary structures, and 4) are responsible for resolving misfolded protein after exposure to cellular stress. The chaperone family includes a large subclass of stress response proteins called heat shock proteins (HSPs), primarily categorized by molecular weight, with the major classes being 40 kDa heat shock proteins (HSP-40s), 60 kDa heat shock proteins (HSP-60s), 70 kDa heat shock proteins (HSP-70s), and 90 kDa heat shock proteins (HSP-90s). All of the chaperones are capable of preventing aggregation, but can be further distinguished between those that require ATP for activity and bind the ribosome, those that bind only ATP, those that only bind the ribosome, and those that aid folding without requiring ATP or binding to the ribosome. In most cases, though, association with the chaperone complex is driven by ATP binding and subsequent hydrolysis providing energy for the process. This is true of both molecular chaperone classes HSP-60 and HSP-70 (Caplan, Cyr, & Douglas, 1993; Fink, 1999).

The HSP-60 family of molecular chaperones includes large barrel-shaped protein complexes called chaperonins. The most extensively studied of these chaperonin systems is the GroEL/GroES chaperonin system in *E. coli*. GroEL is a two protein double ring complex with an ATP-ase domain that forms a barrel-like structure that allows for proper folding of over 250 cytosolic proteins. The unfolded intermediates are shielded from other cellular components, including other folding proteins, within the walls of the GroEL/GroES complex shielding the unfolded protein in an environment conducive to unfolding and refolding. Upon binding of ATP to GroES, the wall of the complex becomes highly hydrophilic allowing for proper folding of the tertiary structures within

(Vabulas et al., 2010).

The HSP70 family of molecular chaperones also requires hydrolyzing ATP activity. The HSP70 family is an extensive class of proteins with a highly conserved ATP binding site and COOH-terminal domain for peptide binding that are regulated by another family of chaperones, HSP-40s (Fink, 1999). A subset of these HSP-70/HSP-40 complexes associates with ribosomes. During protein translation these complexes are abundant and both bind the large ribosomal subunit and interact with the nascent polypeptides (Koplin et al., 2010). With the exception of certain archaea, all cells possess both constitutively produced and stress-induced HSP70/HSP40 complexes. The most extensively studied of these systems include: the mammalian HSC70; a constitutive cytosolic member, HSP70; a cytosolic form induced by stress, HSP-4/BiP/GRP78; an endoplasmic reticulum specific form, and mHSP70; a mitochondrial form. In *E. coli,* DnaJ and DnaK are the bacterial equivalents of the HSP70/HSP40 complex (Caplan et al., 1993). Another system with homologs to the HSP70/HSP40 complex includes the Ssa1-4 and Kar-2 complex in yeast (Shaner, Wegele, Buchner, & Morano, 2005). HSP70 proteins can discriminate between unfolded and folded proteins, but bind only the unfolded intermediates. In these systems, the binding and release of the unfolded protein is dependent on the cycle between ADP and ATP. The exact mechanism of how the HSP70/HSP40 complex interacts with the unfolded substrates has yet to be elucidated (Georgopoulos & Welch, 1993., Hartl, 1996). While a number of chaperones bind to ribosomes and/or require ATP for functioning, there is a subset that requires neither.

The small HSP (smHSP) family comprises proteins ranging from 17 to 30 kDa that do not bind to ribosomes or ATP. These small chaperones all possess a shared

conservative C-terminal domain of the α- crystalline protein typically found in the vertebrate eye lens, though their exact conformations have yet to be identified (Waters, Lee, & Vierling, 1996). Because these chaperones require neither the ribosome, nor ATP, these smHSPs are highly mobile oligomers that vary in composition. smHSPs can be found bound as dimers or in aggregates of over 20 monomers. Many smHSPs are constitutively produced, but a small subset is only expressed during cellular stress. During cell stress, the smHSPs bind hydrophobic regions of misfolded protein to prevent aggregation and establish a temporary reservoir of the misfolded proteins. Once the cellular stress has been resolved, or energy becomes more freely available, the smHSPs transfer the unfolded proteins to ATP-driven chaperones to be degraded or refolded (Mymrikov, Seit-Nebi, & Gusev, 2011; Sun & MacRae, 2005). In plants, the smHSP's gene family determines the transport destination of certain smHSPs. These related smHSPs are responsible for protein transport to the endoplasmic reticulum, mitochondria, cytosol, and chloroplasts (Waters et al., 1996). Though the activity of the smHSPs is not energy dependent, misregulation or deficiencies putatively can lead to much pathology.

The final class of chaperones consists of those that bind the ribosome but do not bind ATP. While many members populate the above classes of chaperones, there is only one chaperone complex known to bind to the ribosome but not require ATP, making it unique among the proteins. The nascent polypeptide-associated complex (NAC) is a conserved chaperone complex that associates with the nascent peptide as it emerges from the ribosome, classifying it as a translational chaperone. The complex is primarily composed of equimolar obligate dimers: one α and one β subunit, although two β subunits have been observed in yeast (del Alamo et al., 2011; Raue, Oellerer, & Rospert.,

2007). The α subunit of the NAC complex interacts with the ribosome via ribosomal subunit RPL25, while both α and β subunits interacts with the emerging peptide (Y. Zhang et al., 2012). The primary known role of the NAC complex is to protect the nascent peptide from protease attack during translation but it has also shown protective potential during cell stress that may be related to a chaperone-like function. During homeostasis in healthy cells, the majority of the NAC is bound to the ribosome (Hetz et al., 2006; Raue et al., 2007). During cellular stress induced by misfolded protein, however, bound NAC is sequestered away from the ribosome and the β subunit appears to bind to the misfolded protein. In this manner, NAC responds to imminent proteotoxic stress and modulates translation until homeostasis is recovered. Once homeostasis is restored, the NAC is sequestered back to the ribosome (Kirstein-Miles, Scior, Deuerling, & Morimoto, 2013). While the exact targets and complete set of functions of the NAC have yet to be fully defined, disruption to NAC function can be costly to the cell and to the organism.

2.2 NASCENT POLYPEPTIDE ASSOCIATED COMPLEX

Under wild-type conditions, nascent polypeptides that interact with the NAC are targeted to cellular compartments that are not the ER; e.g. the mitochondria (Y. Zhang et al., 2012). When faced with non-misfolded protein stress, αNAC is ubiquitinated and degraded, presumably as part of a protective response, but extensive instability of αNAC, and therefore the NAC complex itself, can lead to the mistargeting and mislocalization of proteins to the ER (Hirioshi, 2009). Genetic knockouts of NAC subunits in *C. elegans*, *D. melanogaster* and mice confirm the necessity of the complex for viability, although the association of lethality with various putative functions of NAC is not completely

understood (Bloss, Witze, & Rothman, 2003; Deng & Behringer, 1995; Markesh et al., 2000). In *C. elegans,* removal of the β NAC subunit results in an upregulation of apoptosis, a regulated and conserved cell death process. The upregulation of apoptosis induced by the removal of the β subunit of the NAC is enough to support the role of the NAC as a mediator of apoptosis. Neuronal cells show a particular susceptibility to apoptosis as a result of β NAC depletion in *C. elegans*. Complete knockout of the β NAC sub-unit is embryonically lethal (Bloss et al., 2003). Unlike the above noted metazoans, depletion of the NAC in yeast is not sufficient to induce protein misfolding or any apparent effects on viability. However, in conjunction with a knock down of the HSP70 homologue in yeast, NAC removal results in the aggregation of nascent proteins at the ribosome, as well as decreased viability (Koplin et al., 2010). These findings suggest that the NAC is a salient player in the maintenance of viability, and the prevention of improper protein folding and localization in yeast as well as multicellular organisms.

In its role as a translational chaperone, the NAC was hypothesized to prevent mislocalization of protein to the ER; recent evidence has now proven that depletion of the NAC does indeed result in improper targeting of nascent proteins to the ER. This targeting seems to be at least in part modulated by an interaction with the ER-targeting signal recognition particle (SRP) though the exact mechanism has yet to be defined. The ultimate destination for a nascent protein seems to be modulated cooperatively and or competitively through interactions between SRP and NAC. The SRP recognizes hydrophobic signal sequences on peptides emerging from ribosomes and targets these nascent proteins to the ER (Y. Zhang et al., 2012). Two hypotheses defining the competitive interaction between SRP, NAC and the targeting of nascent proteins have

emerged. The first proposes that the NAC protects a signal-less ribosome/nascent complex from inappropriate interactions. This positions NAC as a negative regulator of SRP, suggesting that NAC sterically prevents binding of SRP (Lauring, Sakai, Kreibich, & Wiedmann, 1995). Conversely, NAC may play a cooperative role for the SRP transport to the ER, for in yeast signal-less ribosome nascent complexes are not translocated to the ER (Y. Zhang et al., 2012). It has also been suggested that NAC binds to non-signal binding ribosomes to prevent mislocation to the ER independent of SRP function. This model is supported by NAC depletion studies that show nascent peptides in NAC (-) cells move to the ER membrane and translocate regardless of bound SRP or signal peptides. Reintroduction of purified NAC is enough to rescue the improper targeting and translocation of proteins to the ER (Lauring et al., 1995). These finding suggest that NAC translocation can be SRP independent. Under the influence of stress conditions associated with aging, bound βNAC is sequestered away from the ribosome and relocalized to accumulating misfolded protein in the cytosol. This chaperone function seems to provide a short term rescue mechanism for the cell, but long term cytosolic usage of NAC may interrupt normal nascent peptide translocation to the ER as well as translation itself, resulting in exacerbated cell stress and even death (Kirstein-Miles et al., 2013).

While no links between viability and removal of NAC have been found in yeast, depletion of the NAC in conjunction with depletion of an hsp70/hsp40 ATP-binding chaperone, stress70b (SSB) results in decreased cell viability and an increased presence of protein aggregates. SSB, like NAC, binds both the nascent chain and the ribosome associated-complex (RAC) and their similar functions are reflected both spatially and in

their ability to induce additional chaperone activity, though SSB, unlike NAC, does require ATP (Koplin et al., 2010). Similarly, improper targeting of the nascent proteins due to depletion of the NAC is enough to trigger upregulation of the ER specific hsp70 chaperone BiP/GRP78 homologue HSP-4 in *C.elegans* (Arsenovic, Maldonado, Colleluori, & Bloss, 2012). HSP-4 expression alone can be enough to resolve low levels of misfolded protein stress in the ER (Nishikawa, Brodsky, & Nakatsukasa, 2005). If homeostasis is not re-established or should misfolded protein stress persist, prolonged requirement of HSP-4 as a chaperone results in the activation of the Unfolded Protein Response (UPR); an ER specific stress-response program in eukaryotes exhibited during misfolded protein stress (Arsenovic et al., 2012).

HSP-4, like other hsp70 homologues, recognizes hydrophobic regions of misfolded proteins that are normally buried within the conformation. Once recognized, HSP-4 employs ATP dependent processes to facilitate refolding. In cases of a prolonged presence or a high concentration of aberrant proteins, HSP-4 is sequestered from bound ER membrane proteins to misfolded protein with high affinity, where they are then targeted for ER-associated protein degradation (ERAD). Proteins targeted for ERAD are translocated from the ER to the cytosol to be ubiquitinated and degraded. HSP-4 is required for all ERAD translocation which in turn results in reduced concentration of misfolded proteins in the ER (Nishikawa et al., 2005). As stated earlier, prolonged chaperone activity exhibited by HSP-4 activates the Unfolded Protein Response (UPR); a conserved cellular mechanism essential to an organism's viability due to its role in embryonic cell differentiation, responses to viral and microbial infections, and combating age related protein stresses. The primary goal of the UPR is to clear the ER of misfolded

protein. As a component of this response, the ERAD is engaged to degrade misfolded protein, but the UPR provides a more global response to protein stress as well. To prevent continued polypeptide influx to the ER, the UPR suppresses general gene transcription and translation, including the expression of secretory proteins, while the translation of chaperones and foldases are concomitantly increased. ER membrane biogenesis is also increased as a means to expand the ER, allowing for the dilution of misfolded protein concentration and providing room for increased chaperone activity in the previously compact space. Finally, should the stress not pass, the UPR has the ability to kill cells, through both pro-apoptotic and pro-autophagic mechanisms.

2.3 THE UNFOLDED PROTEIN RESPONSE IN *C. eLEGANS*

Three ER resident transmembrane proteins; inositol-requiring protein-1 (IRE1), protein kinase RNA (PKR) -like ER kinase (PERK/PEK-1), and activating transcription factor-6 (ATF6) initiate UPR signaling in worms. Each of these proteins defines a distinct arm of the UPR. All of these proteins possess an ER lumenal domain that senses protein load and misfolding in the ER through their interaction with HSP-4; they also contain a cytoplasmic domain that initiates the stress response-signaling cascade. During homeostasis, the UPR proteins are bound by HSP-4 and thereby held inactive. During misfolded protein stress, however, HSP-4 binds the aberrant proteins with high affinity, releasing the UPR elements for activation. Once the stress has been resolved, HSP-4 rebinds the UPR components, rendering them inactive to abrogate the response (Bertolotti, Zhang, Hendershot, Harding, & Ron, 2000; Nishitoh et al., 2002; Shen, Ellis, Sakaki, & Kaufman, 2005).

The most highly conserved arm of the UPR is IRE1, present from yeast through

humans. IRE1, like the other UPR arms, is an ER resident transmembrane protein with a lumenal domain, and a cytoplasmic region containing a kinase domain. Once HSP-4 is sequestered to misfolded protein, unbound IRE1 monomers move laterally along the ER membrane and oligomerize with each other, though the exact mechanism is not known. Oligomerization of IRE1 results in autophosphorylation of the cytoplasmic portion of the IRE1, conferring an allosteric change that stimulates its endoribonucleolytic activity (Sidrauski & Walter, 1997). Once activated, IRE1 behaves as an endonuclease, spliceing a 26-base pair fragment out of the mRNA that encodes the transcription factor HAC-1 (homologous to ATF/CREB1) in yeast, and XBP-1 (X-Box Binding Protein-1) in most other metazoans (Cox & Walter, 1996)Mori, 1996. (Calfon et al., 2002; Yoshida, Matsui, Yamamoto, Okada, & Mori, 2001). This splicing event results in a frame shift that generates an isoform of HAC-1/XBP-1 responsible for upregulating specific UPR genes including those that promote ERAD and ER biogenesis (Yoshida et al., 2003). In yeast, the un-spliced isoform of HAC-1 represses the translation of proteins required during UPR, while the spliced isoform allows for the translation of these proteins. In higher eukaryotes, both the un-spliced and spliced isoforms of XBP-1 are translated, indicating a more complex level of regulatory function. Here, the spliced form of XBP-1 is more stable relative to its un-spliced version, and serves as an upregulator of UPR-specific gene expression. As the UPR resolves the misfolded protein stress in the ER, IRE1 becomes inactivated, resulting in translation of the un-spliced form of XBP-1. Unspliced XBP-1 represses the expression of the genes targeted by the spliced isoform of XBP-1, thereby mitigating IRE-1's contribution to the UPR (Yoshida, Oku, Suzuki, & Mori, 2006).

Short term activation of IRE1 results primarily in the processing of XBP-1 and the subsequent upregulation of UPR genes meant to rescue the cell from stress; chronic activation of IRE-1 eventually engages a second, independent pathway that can lead to the death of the cell. In mammals, prolonged IRE1 activation leads to the recruitment of tumor necrosis factor receptor (TNFR)-associated factor-2 (TRAF-2) to IRE-1. The interaction between TRAF2 and activated IRE1 activates Jun N-terminal kinase (JNK), triggering a stress induced apoptotic pathway (Gabai, Meriin, Yaglom, Volloch, & Sherman, 1998; Ozcan et al., 2004). Additionally, the TRAF2/IRE1 complex has been shown to activate caspase-12 independently of JNK activity, consistent with the initiation of apoptosis (Yoneda et al., 2001). Unlike many other caspases, caspase-12 is ER specific and is active only during ER stress. Mice deficient in caspase-12 show initial resistance to ER stress induced apoptosis, but eventually die by alternatively induced apoptosis, supporting the argument that redundancies in ER-induced apoptotic signaling exist (Nakagawa et al., 2000). In mammals, immunoprecipitation assays suggest an interaction between the IRE1α (one of two mammalian IRE homologues: IRE1αand IRE1 β) and Bak and Bax, pro-apoptotic proteins that modulate mitochondrial apoptosis, potentially linking IRE1-induced apoptosis initiating from the ER with apoptotic pathways that target the mitochondria (Hetz et al., 2006). These findings suggest that IRE1 plays a crucial role in UPR management through the regulation of both cell-saving and cell-killing mechanisms in response to misfolded protein stress.

In addition to stress management, IRE1 also appears to play a significant role in differentiation; whether this role employs the same UPR mechanisms is not known. IRE1, however, does seem to be involved in many tissues that are secretory in nature. In

mammals, two homologues of IRE1, IREα and IRE β, vary in both when and where they are expressed. IRE1α is ubiquitously expressed, while IRE1β is expressed solely in the intestinal epithelium. UPR signaling and splicing of XBP-1 are controlled by the IRE1α homologue. Suppression of the IRE1α's endonuclease activity, however, does not interrupt the cell's response to ER stress, but does inhibit ER biogenesis in exocrine cells. Since only IREα is affected by routine ER stress, but inhibits cell generation, it is likely that IRE1α may more significantly contribute to differentiation than its homologue, IRE1 β (Cross et al., 2012; Kaufman et al., 2002; Scheuner et al., 2001). IRE1α, the ubiquitously expressed form of IRE-1 in many organisms, is essential for the development of the pancreas in *Xenopus laevis* (Yuan et al., 2014), the differentiation of the epithelium of the esophagus and chondrocytes in mice (Rosekrans et al., 2014;Guo et al., 2014), and the differentiation of photoreceptors in *Drosophila melanogaster* (Coelho et al., 2013). IRE1α promotes these differentiation activities through both XBP-1-dependent and independent pathways (Coelho et al, 2013), and knockouts of either IRE1α or XBP-1 results in early embryonic lethality at a similar age relative to one another in mice (Reimold et al., 2000; K. Zhang et al., 2005), indicating that both pathways may be important for cell differentiation during the same stage of embryogenesis.

The second arm of the UPR is PERK/PEK-1. PERK is an ER localized transmembrane protein with a lumenal stress-sensing domain similar to the corresponding domain of IRE1. Also like IRE1, PERK's cytoplasmic portion contains a kinase that is activated via oligomerization and subsequent-autophosphorylation in the ER membrane (Bertolotti et al., 2000). Unlike IRE1, whose only known target of phosphorylation is a

proximal IRE-1 kinase, activated PERK phosphorylates the α subunit of eukaryotic translation initiation factor-2 (eif2α). Phosphorylation of eif2α results in a decrease in the efficiency of mRNA binding to ribosomes, resulting in a global reduction of translation, thus reducing additional protein folding stress on the ER. While this event reduces the translation of most mRNA in the cell, it increases the relative efficiency of translation of a select set of mRNAs whose protein products contribute to the UPR response, in particular ATF4. ATF4 translocates to the nucleus and increases translation of transcription factor CC/EBP homologous protein (CHOP), whose target genes control growth arrest, apoptosis, and autophagy (Marciniak et al., 2004). Though PERK has been linked to ATF4-associated transcription, studies in mammalian cells show that only half of UPR genes modulated by PERK are ATF4-dependent, suggesting that PERK regulates the expression of other UPR players independently of ATF4, though how PERK does this is unknown (Ron & Walter, 2007). Once ER stress has been resolved, PERK is dephosphorylated and inactivated within minutes (Bertolotti et al., 2000). Similar to IRE1, PERK can help save stressed cells, in this case by reducing translation. But also like IRE-1, in cases of prolonged ER stress, PERK has the potential to trigger cell death, in part through the upregulation of the transcription factor CHOP and the pro-apoptotic genes controlled by CHOP activity. The final arm of the UPR is metazoan-specific ATF6. Like PERK and IRE1, ATF6 has a transmembrane portion and a luminal stress-sensing domain, while its cytosolic moiety contains a basic leucine zipper (βZIP) transcription factor. Unlike PERK and IRE1, however, once activated, ATF6 does not oligomerize but instead translocates to the Golgi Apparatus (Chen et al., 2002). There, ATF6 is cleaved by site 1 protease (S1P), and site 2 protease (S2P), releasing the DNA

binding portion of ATF6 (Haze, Yoshida, Yanagi, Yura, & Mori, 1999; Ye et al., 2000). Once released, this moiety translocates to the nucleus, where it acts as a transcription factor that activates expression of ER-specific chaperones as well as XBP-1. ATF6, unlike IRE-1 and PERK/PEK, does not seem to have pro-apoptotic functions; instead, ATF6 only functions to enhance and expand the cell-saving aspects of the UPR (K. Zhang et al., 2005). ATF6 knockout mice are not embryonically lethal, but do show a susceptibility to ER stress, supporting ATF6's role as non-essential modulator of the UPR without the putative role(s) in differentiation that IRE-1 and PERK may perform (Wu et al., 2007, Yamamoto et al., 2010).

2.4 AUTOPHAGY

While the main goal of the UPR is to eradicate ER stress and reinstate homeostasis, often times the cell cannot reverse the cellular stress adequately. In a final survival attempt, a subset of cell types resort to a less robust form of protein aggregate removal, called autophagy. Autophagy degrades misfolded proteins and damaged organelles via double membrane bound vesicles called autophagosomes. Once formed, autophagosomes sequester cytosolic proteins and fuse with a lysosome, where the autophagosomes contents are degraded (Levine and Klionsky, 2004, Yorimoto and Klionsky, 2005). Increased formation of autophagosomes has been associated with ER stress. Depletion of either IRE1 or XBP-1 is known to block autophagy, and results in reduced cellular viability (Yorimitsu et al., 2006). Unfortunately, much is still to be learned about the induction of autophagy by ER stress. Due to the energetic expenditure and transcriptional modulation, it is likely that autophagy is engaged prior to apoptosis in a final attempt to save the cell from death. Autophagosomes are associated with

increased viability if associated with short term ER stress, but increased exposure results in death regardless of autophagic responses (Ogata et al., 2006). Consistent with this conclusion, both IRE-1 and PERK initiate protective responses during early cell stress, but the extended stress results in accompanying increased activities of JNK and CHOP respectively, both of which are potent initiators of apoptosis.

2.5 APOPTOSIS

As noted, the role of the UPR in cells too damaged to save is to initiate apoptosis. Apoptosis is a highly conserved evolutionary process that results in the organized disintegration of unnecessary or damaged cells in multicellular organisms. Unlike necrosis, an unregulated and destructive form of cell death by comparison, apoptosis plays an essential role in the maintenance of a healthy organism when properly regulated. Cells that are fated to die by intrinsic or extrinsic signals undergo chromosomal condensation and are systematically fragmented and engulfed by neighboring cells. This reabsorption of cellular components not only results in a conservation of nutrients but also protects neighboring cells from the toxic cellular components e.g. proteases (Conradt & Xue, 2005).

Apoptosis must remain properly regulated throughout the course of an organism's lifespan; inappropriate regulation can lead to dysfunction and disease. Initially, apoptosis performs a pivotal role in embryonic development, during which, it removes extraneous cells that often served as scaffolding structures while organs mature. This premeditated disposal of cells allows a directed molding of migrating cells to form functional tissues and organs. Apoptosis is also responsible for the removal of vestigial structures that remain present throughout development but serve no known function for the adult

organism, e.g. the webbing found between fingers and toes during human fetal development (Kim & Sun, 2011).

In the adult organism, the role of apoptosis shifts towards the maintenance of homeostasis. To maintain a healthy individual, it is necessary to dispose of cells that become dysfunctional through age and/or endanger the viability of the organism. Potentially dangerous cells that apoptosis typically removes include: old and deteriorating cells, cells in which DNA damage has resulted in loss of viability of organelles, cells that are dividing uncontrollably due to malignancy, and cells that have lost communication with the surrounding environment (Conradt & Xue, 2005).

Mis-regulation of apoptosis can produce a multitude of pathogenic responses linked to disease. In any given cell, mechanisms that control apoptosis integrate with both external and internal stress signals to determine the fate of the cell. The inability to maintain this intricate balance between life and death can result in inappropriate cell loss, leading to neurodegeneration, autoimmune diseases, and retinal degeneration (Jellinger, 2009). Misregulation of apoptosis can also result in failure to induce apoptosis in damaged cells, resulting in tumor formation and progression, as well as infectious pathogenesis due to failed elimination of infected cells. The ramifications of mis-regulated apoptosis necessitate a fundamental understanding of this process to elucidate the role of this mechanism in prevention of disease. As it relates to misfolded protein stress and the UPR, our understanding of how apoptosis is triggered by the UPR is core to our understanding of those elements that determine the "tipping point" of the UPR outcome: cell survival or cell death. As such, these studies should help define the specific conditions in which the UPR triggers death, providing insights into conditions that link

inappropriate UPR activity to disease.

2.6 EXPERIMENTAL STRATEGY AND PREDICTIONS

The focus of my thesis project is to define the relationship between different elements of the UPR and measurable outcomes of UPR signaling, specifically in the context of misfolded protein stress induced by loss of the NAC. Since removal of the NAC has been shown to upregulate the UPR-responsive chaperone, HSP-4, indicating the generation of misfolded protein stress in the ER, I investigated the relationship of the NAC with the UPR by depleting *C. elegans* embryos of the NAC induced ER stress proteins in diminished UPR backgrounds. To perform these analyses, I used the model system *C. elegans*, a well-characterized and genetically malleable nematode with a highly conserved UPR and NAC. Using RNA interference for both *icd-1* and *icd-2*, I examined four UPR knockout worms (IRE1, XBP-1, PERK and ATF6) progeny to evaluate how NAC removal induces ER stress, and how that ER stress is managed without specific elements of the UPR. In order to get a more global perspective of the RNA i*cd-1* and *icd-2* subunits were depleted individually in all UPR knockout strains, and subsequent progeny was scored based on morphology, number of apoptotic cell corpses, early embryonic lethality, and the presence of bioluminescent lysosomes in gut cells. Through these experiments, I began to determine which elements of the UPR are contributing the stress-response outcomes induced upon depletion of the NAC. These experiments also begin to define NAC as a modulator of UPR responses.

3. METHODS

3.1 MAINTENANCE OF C. ELEGANS WORM STRAINS

C. elegans strains were maintained at 22^{o}C on Nematode Growth Agar (Carolina Biological) seeded with OP50-1 bacteria, an *E. coli* strain auxotrophic for uracil and containing resistance to streptomycin. OP50 feeder was cultured overnight shaking at 37^{o}C in liquid LB Broth containing 50ug/ml streptomycin. Overnight cultures were derived from single colonies streaked from frozen stocks. Worms were transferred to new plates every two to four days to maintain growth. The worm strains maintained were: N2 (wild type); *ire-1*(ko) (SJ30); *xbp-1*(ko) (SJ17); *pek-1*(ko) (RB545) and; *atf6* (ko) (RB772). All strains as well as OP50-1 bacteria were supplied by the Caenorhabditis Genetics Center (CGC, University of Minnesota).

3.2 MOUNTING *C. ELEGANS* FOR MICROSCOPIC ANALYSIS

Embryos from RNAi-treated or control worms were mounted onto agar pads (5% agar in dH_2O) formed on a glass slide and containing 9-10uL of M9 buffer (22 mM KH2PO4, 42 mM Na2HPO4, 86 mM NaCl, 1 mM MgSO4.7H2O). Embryos were distributed evenly across the agar in the M9, and a cover slip was added.

3.3 RNA INTERFERENCES ASSAYS

RNA interference assays were used to inhibit the translation of specific mRNAs for *icd-1*, *icd-2* or *unc-22*. To induce an RNAi response, worms were fed bacteria expressing double stranded (ds) RNA complementary to the mRNA targeted for translational inhibition. dsRNA expression was controlled from a plasmid containing an isopropyl-1-thio-b-D-galactopyranoside (IPTG)-inducible promoter system (Addgene).

Engineered feeder bacteria were grown from single colonies in 25mL of liquid LB by shaking overnight at 37^{o}C. During the last 4 hours of shaking, IPTG was added to the overnight concentration to a final concentration of 10 uM. Cultured feeder bacteria were seeded onto RNAi plates. RNAi plates were made by combining 4.5g NaCL, 25.5g agar, 3.75 peptone, 1.5mL of 2 mg/mL uracil, 0.22 CaCl 0.75g of 10 mg/mL cholesterol in 1463 of dH_2O. This mixture was autoclaved, allowed to cool, and 37.5 mL of phosphate buffer (pH 6), 1.5 mL MgSO4, and 1.5mL of 25 mg/mL ampicillin was added. Also added was IPTG to a final concentration of 2M, 1M or 0.5M depending on the experiment. Seeded plates were dried at room temperature for 24 hours at 20^{o}C.

3.4 ANALYSES OF UPR-DEFICIENT EMBRYOS DEPLETED OF ICD-1 OR ICD-2.

30 young adult worms deficient for an element of the UPR were moved to *icd-1 or icd-2*(RNAi) plates, and their resulting progeny were monitored over a 72 hour period at 20^{o}C. Embryos were taken randomly from worm plates, mounted on agar pads in M9 solution, and viewed on a Zeiss Axioskop using a 100x plan-neofluar objective (N.A 1.3) with immersion oil. Embryos were viewed using DIC optics and Axiocam camera (software: Axiovision). All image's histograms were adjusted. Embryo profiles were generated by classifying embryos phenotypically as 1) wild-type, 2) comma stage, 3) mutant or 4) pre-comma vacuolated. In addition, the relevant embryos were quantified for comma stage apoptosis and evaluated for the presence of lysosomes in intestinal cells. Profiles were used to determine the effect of the RNAi by comparing the embryos development, viability and morphology at different time points during the RNAi. The purpose of profiling embryos was to 1) ensure the RNAi was affecting worms and 2)

make comparisons between wild-type and UPR mutant populations. *unc-22*(RNAi) was used as a control and scored for apoptotic cell corpses. The experiment was duplicated at least three times for each UPR mutant analyzed.

3.5 EMBRYONIC CELL CORPSE ANALYSIS

The number of cell corpses in embryos observed at the comma stage of embryogenesis (~300 minutes post-fertilization) was determined by using Nomarski optics. Corpses were identified by their hallmark separation from surrounding cells and "button-like" morphology. For corpse quantification, only corpses of a normal size and shape were counted. All data are reported as the mean +/- one standard deviation.

3.6 DETERMINATION OF MORPHOLOGICAL DEFECTS AND LARVAL VIABILITY IN EMBRYOS

Morphological defects in experimental embryos were determined based on the state of embryonic structures as well as the state of individual cells within the embryo. Embryos early in development were considered mutant if they displayed dramatic increases in apoptosis and/or necrosis relative to wild type embryos of the same stage, and were classified as "pre-comma vacuolated." Embryos early in development deemed mutant were also scored as terminal with regards to larval viability; these embryos were not expected to hatch into larvae. Embryos late in development were considered mutant if they displayed dramatic increases in apoptosis and/or necrosis and/or showed misshapen body structure relative to wild type embryos of the same stage. Embryos late in development deemed mutant were scored as viable; these embryos were expected to hatch into larvae.

3.7 SEMI-QUANTITATIVE ANALYSIS OF LYSOSOMAL PRESENCE

Embryos were evaluated semi-quantitatively for the number and size of lysosomes present in intestinal cells during NAC-depletion experiments. The state of lysosomal presence in experimental embryos was determined by comparing both the number and size of lysosomes observed in the intestinal cells with the number and size of lysosomes in untreated wild type embryos. Lysosomes were identified via Nomarski optics by their birefringent and almost reflective nature and hallmark, donut-like structure.

4. RESULTS

To elucidate the relationship of the NAC with the UPR during stress, I performed a series of NAC depletion experiments in animals deficient for different UPR elements and measured the effects on stress-induced outcomes during embryogenesis. Previous data from our lab revealed that depletion of *C. elegans* β-NAC homologue ICD-1 was sufficient to trigger up-regulation of *hsp-4* chaperone gene expression, consistent with the induction of ER stress. In order to fully elucidate the role of the NAC complex as an inducer and possible regulator of the unfolded protein response, L4 larval *C. elegans* were depleted of ICD-1 *and* ICD-2 individually in four UPR knock-outs (PERK, ATF6, XBP-1 and IRE1). All results are presumed to be due to depletion of either *icd-1* or *icd-2*, as UPR knockout mutants were unaffected by *unc-22* RNAi controls with respect to the stress-induced outcomes I measured (data not shown).

4.1.1 DEPLETION OF ICD-1 in IRE1 KNOCKOUT WORMS

Late larval IRE1 knock out worms were depleted of *icd-1* using an RNAi feeder strain induced to express double stranded RNA with 2M IPTG. The worms depleted of ICD-1 developed slowly compared to both untreated IRE1 populations and wild-type strains. All worms from this treatment were sterile, produced no embryos, and exhibited protruding vulva. Worms in this treatment were short and distended, and were slow moving. The absence of progeny made assessment of stress-induced phenotypes impossible. Due to the adverse effects of 2M IPTG induced *icd-1* RNAi on viability and sterility; reduced concentrations of IPTG were used. Late larval IRE1 knock out worms were depleted of *icd-1* using either 0.5M or 1M IPTG induced RNAi. Larvae treated

with both treatments were slow to develop, but remained fertile. Embryos produced by these worms were then scored for: the presence of apoptotic cell corpses, effects on embryonic morphology, lysosome presence, and cell viability (Figures 1 and 2).

4.1.2 APOPTOSIS IN IRE1 KNOCK OUT WORMS DEPLETED OF ICD-1

During *C. elegans* embryogenesis, physiological apoptosis occurs as part of normal developmental processes. This invariant process eliminates 131 cells, and is most active at the midpoint of embryogenesis, otherwise known as "comma stage". During this stage, wild-type embryos display, on average, 5 corpses (data not shown), while stressed embryos will display an increased number of corpses depending on the nature and severity of the stress. The initial phenotype observed in ICD-1 depleted embryos was an increase in comma-stage apoptosis, an outcome phenocopied by depletion of ICD-2 (Arsenovic et al., 2012; Bloss et al., 2003). As such, an increase in embryonic apoptosis phenotype is an effective and reproducible measure of NAC depletion in *C. elegans*. To determine the putative contributions of UPR elements on this NAC-depletion phenotype, I observed comma-stage apoptosis in UPR mutants depleted of ICD-1. With regards to worms deficient in IRE-1, embryos produced by worms depleted of ICD-1 using either 0.5M or 1M IPTG exhibited similar levels of comma-stage apoptosis (Figures 1A and 2A). Of the 130 embryos observed from 0.5M IPTG induced RNAi, 20 comma stage embryos had an average of 8.33 cell corpses (Standard deviation ± 2.44) (Figure 1C). Of the 228 embryos observed from 1M IPTG induced RNAi, 46 comma stage embryos had an average of 9.89 cell corpses (Standard deviation ± 3.00) (Figure 3). Embryos in both treatment protocols showed an increase in the number of cell corpses relative to untreated IRE1 knockout embryos (Average= 9.13, Standard deviation ± 2.67) (t test $p<0.05$)

(Figure 3). Apoptotic cell corpses in all cases appeared normal in morphology and general location (Figure 2C).

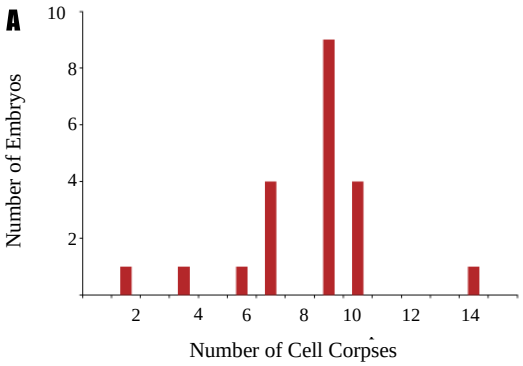
A
Number of Embryos
10
8
6
4
2
2
4
6
8
10
12
14
Number of Cell Corpses

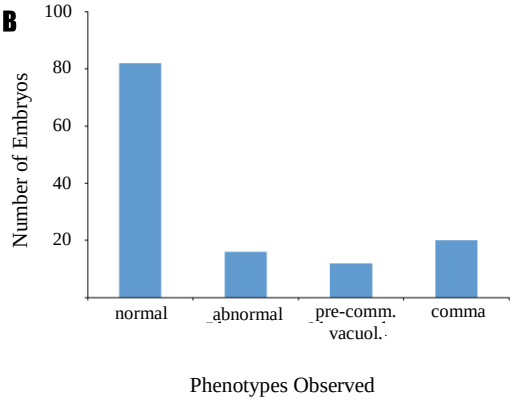
B
Number of Embryos
100
80
60
40
20
normal
abnormal
pre-comm.
vacuol.
comma
Phenotypes Observed

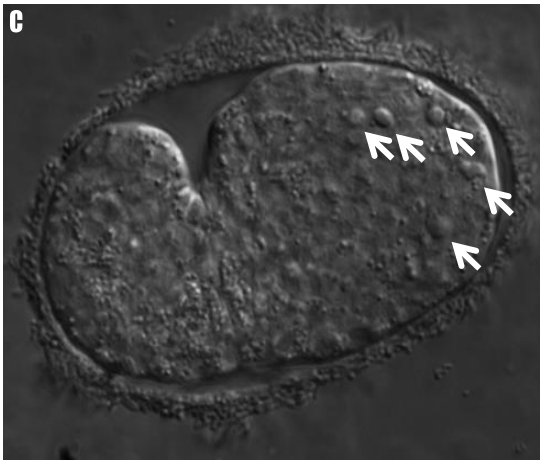
C

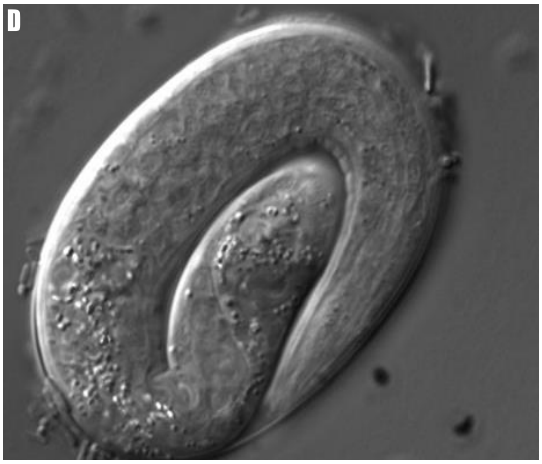
D

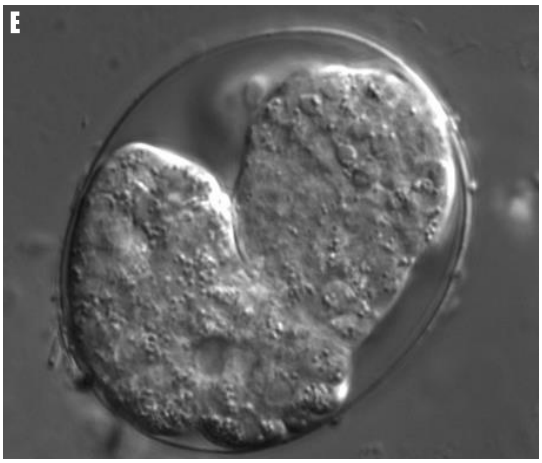
E

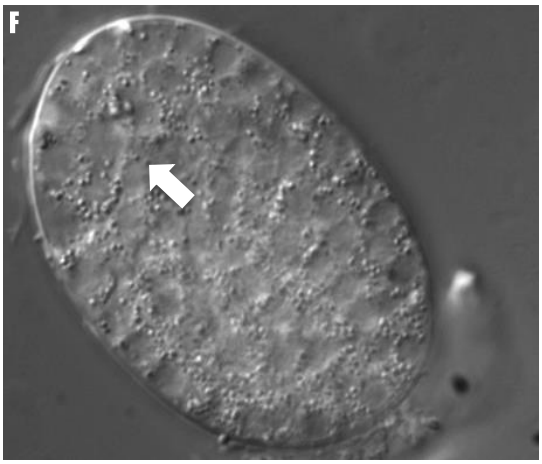
F

Figure 1. UPR effects in *ire-1*(ko) embryos depleted of ICD-1at 0.5M IPTG. *ire-1*(ko) animals were treated with 0.5M IPTG-induced icd-1 RNAi and their progeny characterized for effects on embryonic apoptosis and morphological development. **A)** Quantification of apoptotic cell corpses in *ire-1*(ko) embryos depleted of ICD-1 (n=20). Progeny of ICD-1-depleted worms were scored for the number of corpses assessed at comma stage of embryogenesis (~300 minutes post fertilization). **B)** Quantification of embryonic outcomes in *ire-1*(ko) embryos depleted of ICD-1 (n=130). Embryos were scored as "normal" if they progressed past comma stage displaying normal morphology, as seen in D); embryos were scored as "abnormal" if they progressed past comma stage and displayed mutant morphology, as seen in E); embryos were scored as "pre-comma vacuolated if they arrested prior to comma stage and contained regions of vacuolization, a2s seen in F); embryos were considered "comma" if they were scored at this stage and displayed wild type morphology, as seen in C). **C-F)** Representative progeny embryos from *ire-1*(ko) adult worms depleted of ICD-1. **C)** Representative "comma" embryo displaying button-like corpses indicative of apoptosis (arrows). **D)** Representative "normal" embryo displaying normal morphology, in this case three-fold stage, just prior to hatching. **E)** Representative "abnormal" embryo displaying abnormal morphology, in particular, disruption of the smooth, worm-like structure associated with this stage of development. **F)** Representative "pre-comma vacuolated" embryo displaying a large vacuolated region consistent with the death of epidermal or muscle cells early in development.

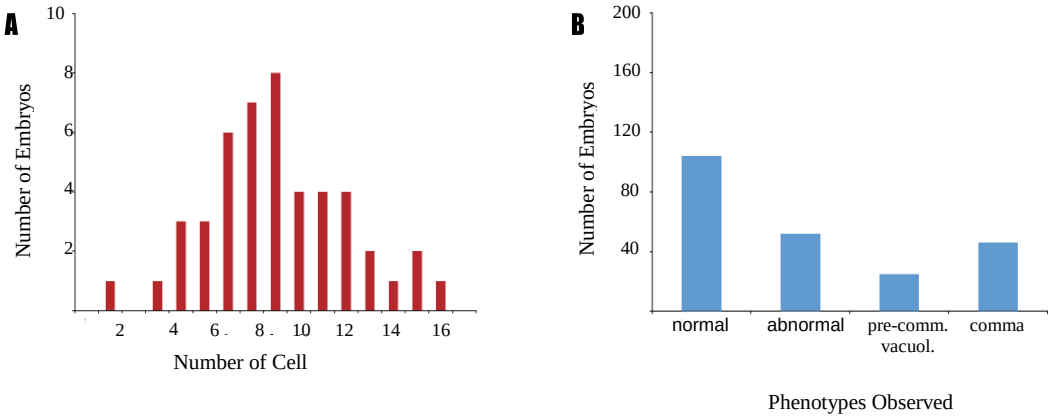
A
Number of Embryos
10
8
6
4
2
2
4
6
8
10
12
14
16
Number of Cell
B
Number of Embryos
200
160
120
80
40
normal
abnormal
pre-comm. vacuol.
comma
Phenotypes Observed

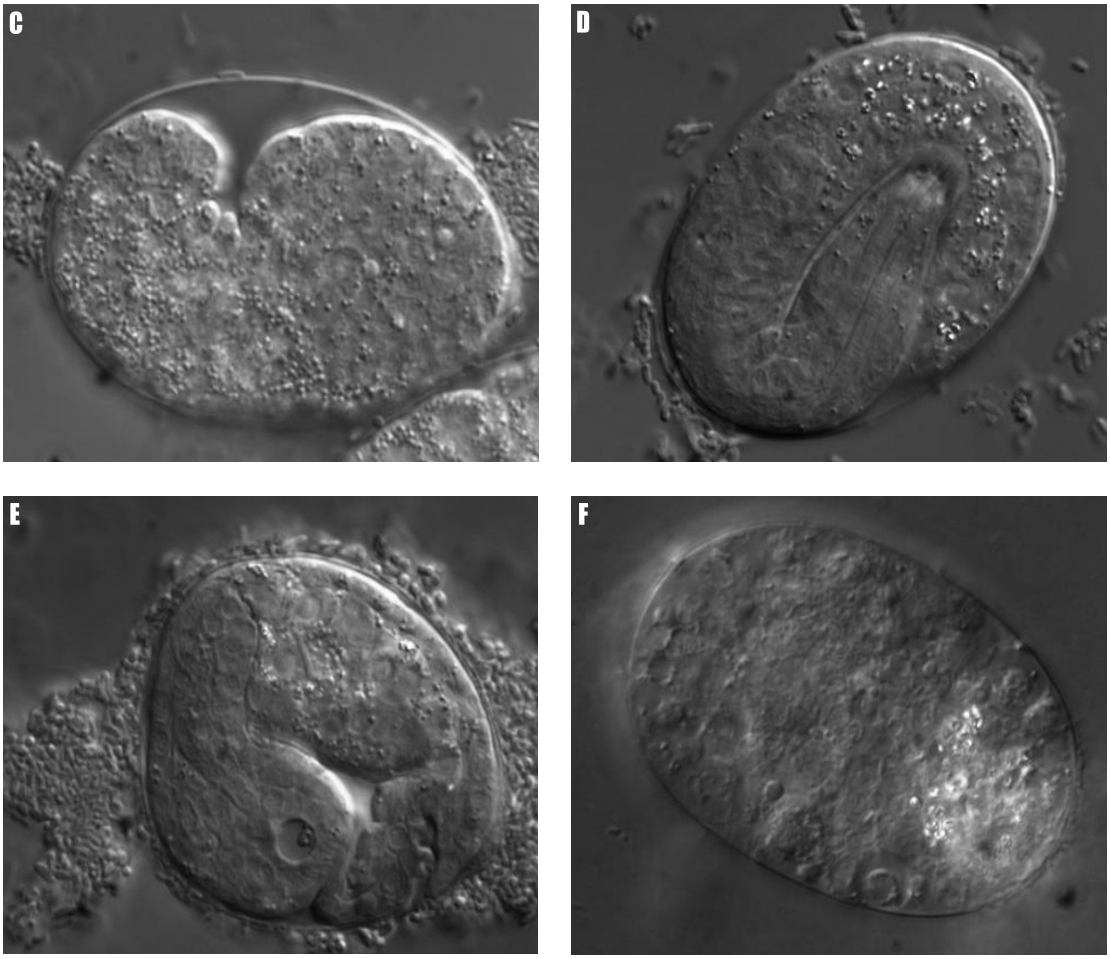
C
D
E
F

Figure 1. UPR effects in *ire-1*(ko) embryos depleted of ICD-1 at 1M IPTG. *ire-1*(ko) animals were treated with 1M IPTG-induced icd-1(RNAi) and their progeny characterized for effects on embryonic apoptosis and morphological development. **A)** Quantification of apoptotic cell corpses in *ire-1*(ko) embryos depleted of ICD-1 (n=46). Progeny of ICD-1-depleted worms were scored for the number of corpses assessed at comma stage of embryogenesis (~300 minutes post fertilization). **B)** Quantification of embryonic outcomes in *ire-1*(ko) embryos depleted of ICD-1 (n=228). Embryos were scored as "normal" if they progressed past comma stage displaying normal morphology, as seen in D); embryos were scored as "abnormal" if they progressed past comma stage and displayed mutant morphology, as seen in E); embryos were scored as "pre-comma vacuolated" if they arrested prior to comma stage and contained regions of vacuolization, as seen in F); embryos were considered "comma" if they were scored at this stage and displayed wild type morphology, as seen in C). **C-F)** Representative progeny embryos from *ire-1*(ko) adult worms depleted of ICD-1.
C) Representative "normal" embryo displaying button-like corpses indicative of apoptosis (arrows). **D)** Representative "wild type" embryo displaying normal morphology, in this case three-fold stage, just prior to hatching. **E)** Representative "abnormal" embryo displaying abnormal morphology, in particular, disruption of the smooth, worm-like structure associated with this stage of development. **F)** Representative "pre-comma vacuolated" embryo displaying a large vacuolated region consistent with the death of epidermal or muscle cells early in development.

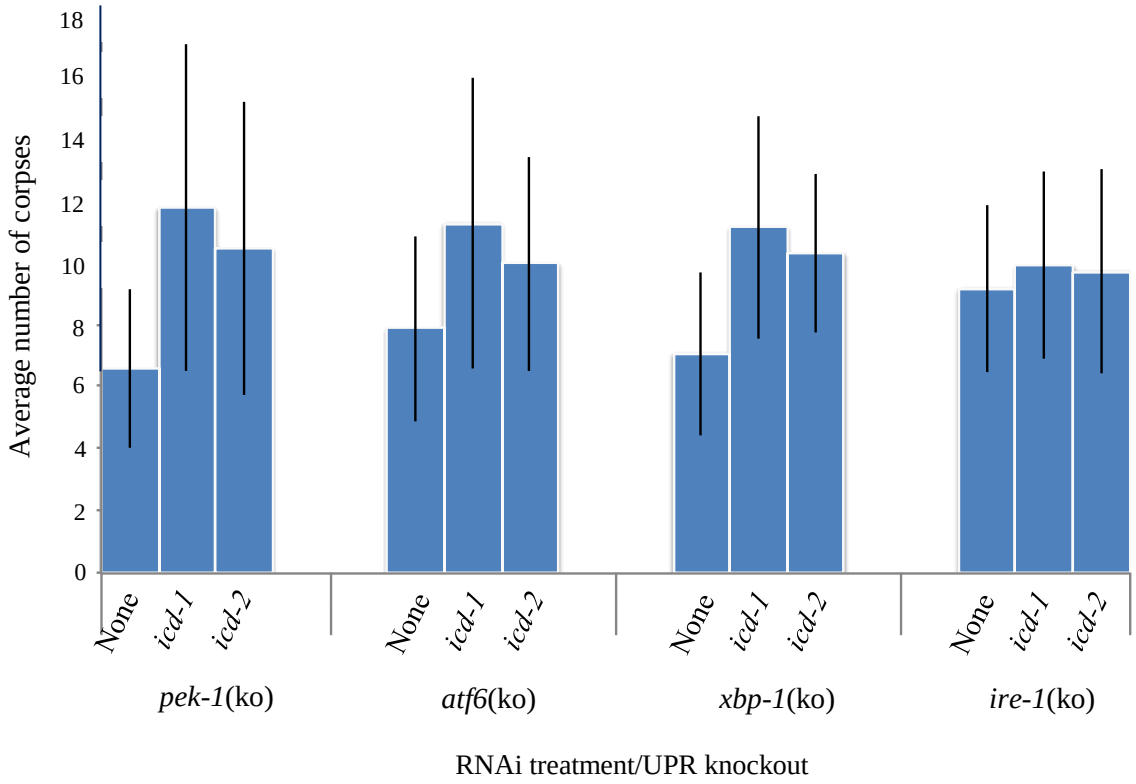

Figure 2. **Average cell corpses observed in UPR-deficient embryos depleted of ICD-1 or ICD-2**. Animals deficient for a specific component of the UPR were depleted via *icd-1* or *icd-2*(RNAi) or received no treatment for 24 to 72 hours at 20^{o}C, and their progeny embryos scored for apoptotic cell corpses. The average number of cell corpses assessed in each mutant background is shown. *ire-1*(ko) embryos were assessed at both 0.5M and 1M concentrations of IPTG and averaged, the chemical used to induce RNA interference in these experiments. Error bars represent one standard deviation from the mean frequency of embryos per UPR-deficient mutant over two or three independent experiments.

4.1.3 MORPHOLOGY IN IRE1 KNOCK OUT WORMS DEPLETED OF ICD-1

In addition to increases in embryonic apoptosis, depletion of ICD-1 or -2 has previously shown significant effects on embryonic morphology, resulting in embryos that appear misshapen and/or vacuolated. To determine any contributions UPR elements might have on the morphology of NAC-depleted embryos, I scored the number of different types of morphologically defective embryos produced by UPR mutant worms depleted of ICD-1.

With regards to IRE-1 knockout animals depleted of ICD-1, of the 130 embryos observed using the 0.5M IPTG protocol, 79% were normal and 21% were morphologically abnormal (Figure 4). Of the 228 embryos observed using the 1M IPTG protocol, 66% were normal and 34% were abnormal. Late stage abnormal embryos collected from both treatments were highly disorganized and often lacked normally identifiable structures (e.g. a clearly defined pharynx and/or gut) (Figure 1E and 2E). Abnormal embryos also exhibited disorganized and rounded protrusions from the embryo consistent with embryos with closure or developmental defects. Many pre-comma embryos were also considered abnormal as they exhibited large vacuolated spaces consistently near the anterior portion of the embryo (Figure 1F and 2F). Both 0.5M and 1M IPTG induced RNAi showed consistent and comparable phenotypes.

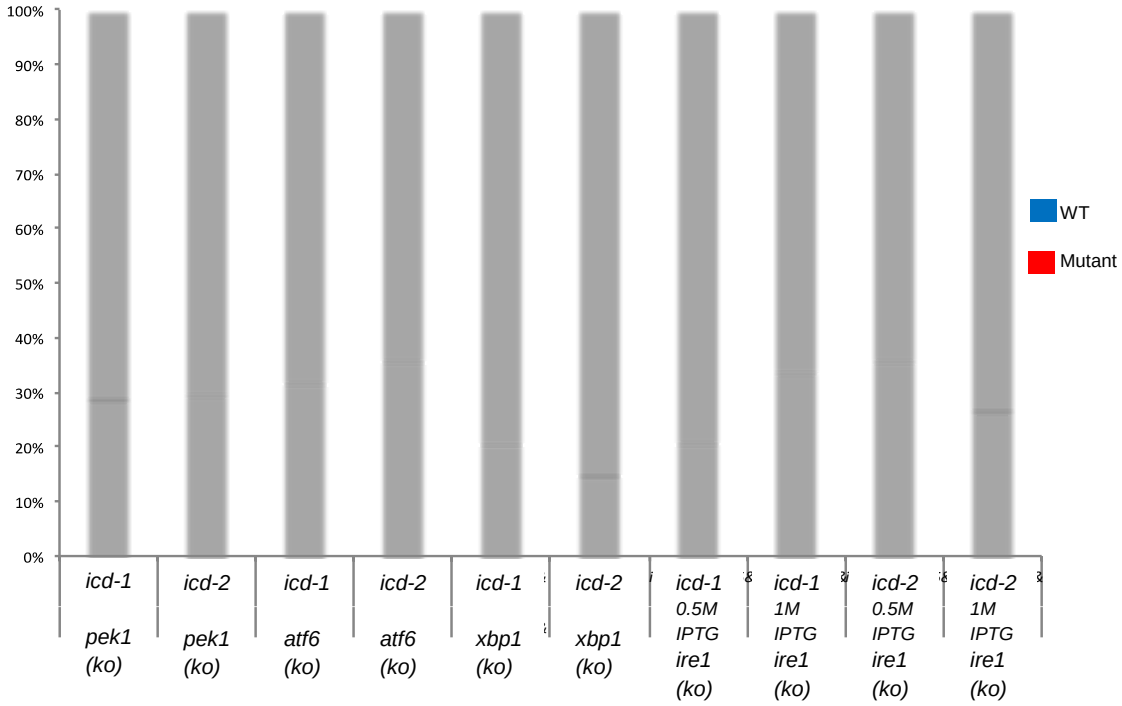

Figure 3. Quantification of embryonic morphologies in UPR-deficient animals depleted of ICD-1 or ICD-2. Animals deficient for a specific component of the UPR were depleted via *icd-1* or *icd-2*(RNAi) for 24 to 72 hours at 20^{o}C, and their progeny embryos scored for morphology. Mutant embryos include those that were post comma and pre-comma vacuolated in nature. *ire-1*(ko) embryos were assessed at both 0.5M and 1M concentrations of IPTG, the chemical used to induce RNA interference in these experiments. At least three independent experiments are represented for each case. Untreated embryos did not exhibit abnormal embryonic morphologies.

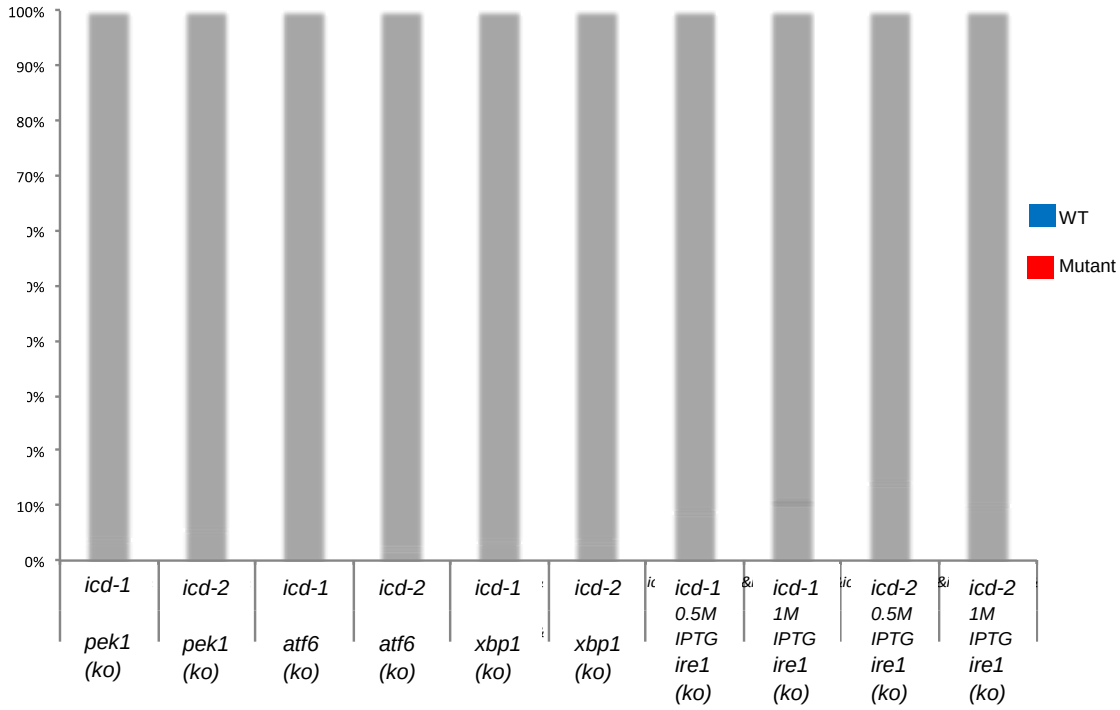

Figure 4. **Quantification of pre-comma vacuolated embryos in UPR-deficient animals depleted of ICD-1 or ICD-2**. Animals deficient for a specific component of the UPR were depleted via *icd-1* or *icd-2*(RNAi) for 24 to 72 hours at 20^{o}C, and their progeny embryos scored for the presence of pre-comma vacuolization. Unlike figure 2, these assessments distinguished post-comma mutant embryos from pre-comma vacuolated embryos. *ire-1*(ko) embryos were assessed at both 0.5M and 1M concentrations of IPTG, the chemical used to induce RNA interference in these experiments. All other experiments utilized 1M concentrations of IPTG. At least three independent experiments are represented for each case. These phenotypes were not observed in untreated animals.

4.1.4 EARLY EMBRYONIC LETHALITY IN IRE1 KNOCK OUT WORMS DEPLETED OF ICD-1

Within the population of embryos deemed morphologically defective, a further distinction was made with regards to the developmental stage of these embryos; those that arrested early in embryogenesis (pre-comma stage), and those that surpassed comma-stage. Historically, NAC-depleted embryos that have progressed past comma stage typically hatch and become larvae, while embryos arrested before comma stage eventually die as embryos. Therefore, the number of early arrested, morphologically defective embryos in a NAC-depleted population deficient for an element of the UPR becomes a reasonable measure of embryonic lethality in that context, and could provide insights into the contribution of the UPR to this stress-induced outcome.

With regards to IRE-1 knockout animals depleted of ICD-1, 9 % of embryos observed in the 0.5M IPTG protocol were scored as early embryonic defective, as they were unable to reach comma stage appropriately (Figure 5 and Figure 4F). Similarly, 11 % of embryos treated with 1M induced IPTG RNAi showed early embryonic arrest. In almost all cases, the embryos showed large vacuolated regions in the anterior portion of the embryo (Figure 2F), and appeared to be at a similar stage of very early development. Both 0.5M and 1M IPTG induced RNAi showed consistent and comparable phenotypes. Due to the similar outcomes, all future experiment were conducted using 1M induced RNAi.

4.1.5 LYSOSOME PRESENCE IN IRE1 KNOCK OUT WORMS DEPLETED OF ICD-1

Depletion of ICD-1 has been shown to induce the up-regulation of the ER-specific chaperone HSP-4 in *C. elegans* embryos, indicating the induction of misfolded protein stress. An additional stress-induced phenotype observed in embryos depleted of ICD-1 is an increase in size and number of lysosomes in gut cells (Arsenovic, 2012). Lysosomes are membrane-bound organelles responsible for the turnover of old or damaged proteins, both in healthy cells and in cells undergoing misfolded protein stress. Increases in misfolded protein levels in the ER are thought to trigger, via the UPR, increases in lysosomal number and size to increase the capacity for protein turnover in the stressed cell. Due to their content, a mixture of proteins and lipids known as lipofuscins, lysosomes are bioluminescent when observed under the microscope, and can therefore be assessed qualitatively. To determine the putative roles elements of the UPR play in the nature of the gut cell lysosomes in ICD-1-depleted embryos, I observed lysosomes in UPR-mutant embryos depleted of ICD-1.

With regards to IRE-1 knockout animals depleted of ICD-1, embryos observed from both 0.5M and 1M IPTG protocols contained numerous large, birefringent lysosomes in their gut cells. Specifically, the embryos most affected were also the embryos with dramatic morphological defects; normal embryos from the same populations showed no noteable increase in lysosomal number or size. The presence of numerous large lysosomes was not restricted by the stage of the mutant embryo; both early and late stage abnormal embryos were found to have increases in lysosome numbers and size (Figure 1D, 2D and 2F).

4.1.6 DEPLETION OF ICD-2 IN IRE1 KNOCK OUT WORMS

Initial studies of the NAC in *C. elegans* have focused primarily on depletion of ICD-1/ β NAC as a way to deplete the NAC itself; if one subunit of the complex is diminished, then levels of the whole complex will also diminish regardless of the level of the other subunit, i.e. ICD-2/ α NAC. Recent findings, however, indicate roles for the individual subunits independent of their work as a complex; roles that may affect the stress-induced phenotypes being observed in my studies. Therefore, to fully understand the relationship between the NAC and the UPR in the context of misfolded protein stress, I determined the effects of ICD-2 depletion on stress-induced outcomes during embryogenesis. Any differences observed between these results and those associated with ICD-1 depletion may provide insights into how the overabundance of one NAC subunit relative to the other may affect the ability of the UPR to manage the misfolded protein stress triggered by the loss of the complex itself.

With regards to IRE-1 knockout animals depleted of ICD-2, late larvae exposed to either 0.5M or 1M IPTG were slow to develop, but remained fertile. I used embryos from these worms to score for the presence of apoptotic cell corpses, effects on embryonic morphology, lysosome presence, and cell viability (Figure 6B and Figure 7B).

4.1.7 APOPTOSIS IN IRE1 KNOCK OUT WORMS DEPLETED OF ICD-2

With regards to worms deficient in IRE-1, embryos produced by worms depleted of ICD-2 exhibited similar levels of comma-stage apoptosis whether using either 0.5M or 1M IPTG (Figures 6 and 7). Of the 228 embryos observed from the 0.5M IPTG

population, 33 comma stage embryos had an average of 8.80 cell corpses (standard deviation ± 2.84). Of the 126 embryos observed from 1M IPTG population, 24 comma stage embryos had an average of 9.68 cell corpses (standard deviation ± 3.28). As with the depletion of ICD-1 in IRE-1 abnormal embryos, depletion of ICD-2 using either treatment protocol did not show an increase in the number of cell corpses relative to untreated IRE1 knockout embryos (t test $p<0.05$) (Figure 3). In all cases, apoptotic cell corpses appeared normal in morphology and location.

4.1.8 MORPHOLOGICAL DEFECTS, EARLY EMBRYONIC LETHALITY AND LYSOSOME PRESENCE IN IRE1 KNOCK OUT WORMS DEPLETED OF ICD-2

As with embryonic apoptosis, depletion of ICD-2 in IRE-1 knockout embryos resulted in stress-induced phenotypes that closely resembled those found in ICD-1-depleted embryos. The percentage of morphologically defective embryos was reduced in ICD-2-depleted embryos relative to embryos depleted of ICD-1, but the difference is not significant, and the morphological defects themselves appeared to be the same. The percentage of early embryonic defective embryos observed within this abnormal population closely resembled that found in ICD-1 depleted embryos, while also displaying the same vacuolated phenotype observed in ICD-1 early arresters. Finally, the general effects on lysosome size and presence in embryos depleted of ICD-2 phenocopies the effects seen upon ICD-1 depletion, again failing to identify a difference in stress-induced phenotypes in IRE-1 knockout embryos depleted of ICD-2 versus those depleted of ICD-1.

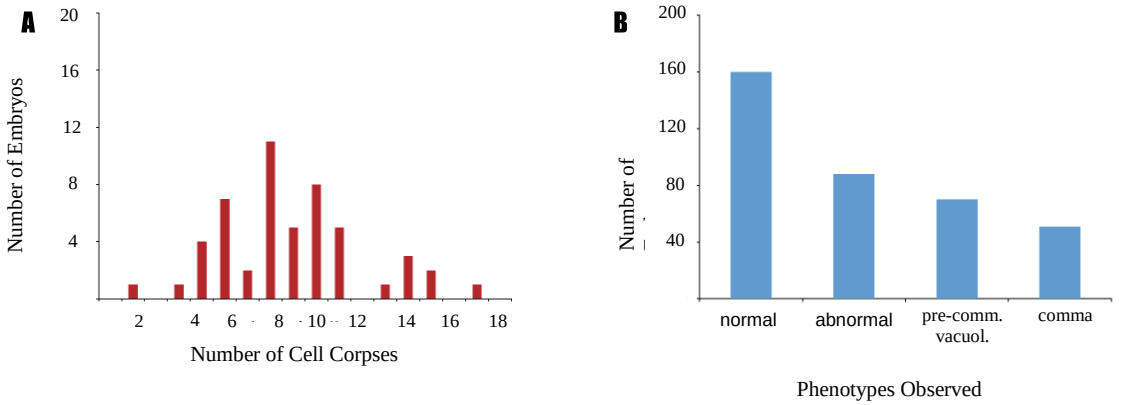
A
Number of Embryos
20
16
12
8
4
2
4
6
8
10
12
14
16
18
Number of Cell Corpses
B
200
160
120
80
40
normal
abnormal
pre-comm. vacuol.
comma
Phenotypes Observed

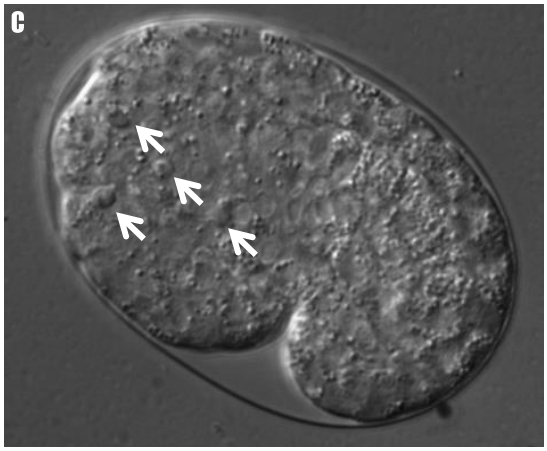
C


D

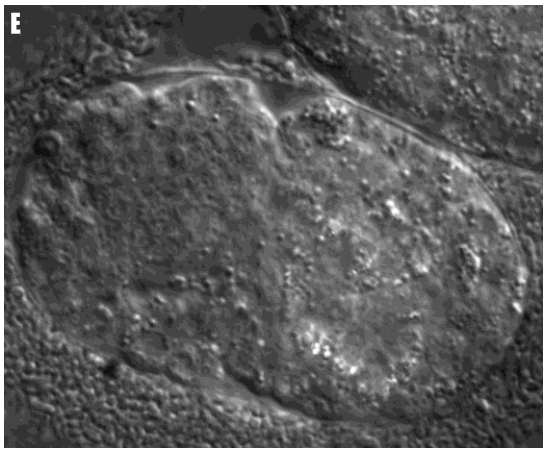
E

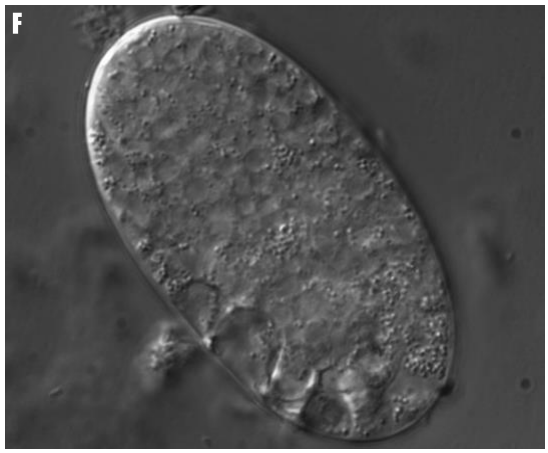
F

Figure 5. UPR effects in *ire-1*(ko) embryos depleted of ICD-2 at 0.5M IPTG. *ire-1*(ko) animals were treated with 0.5M IPTG-induced icd-2(RNAi) and their progeny characterized for effects on embryonic apoptosis and morphological development. **A)** Quantification of apoptotic cell corpses in *ire-1*(ko) embryos depleted of ICD-2 (n=33). Progeny of ICD-2-depleted worms were scored for the number of corpses assessed at comma stage of embryogenesis (~300 minutes post fertilization). **B)** Quantification of embryonic outcomes in *ire-1*(ko) embryos depleted of ICD-2 (n=228). Embryos were scored as "normal" if they progressed past comma stage displaying normal morphology, as seen in D); embryos were scored as "abnormal" if they progressed past comma stage and displayed mutant morphology, as seen in E); embryos were scored as "pre-comma vacuolated" if they arrested prior to comma stage and contained regions of vacuolization, as seen in F); embryos were considered "comma" if they were scored at this stage and displayed wild type morphology, as seen in C). **C-F)** Representative progeny embryos from *ire-1*(ko) adult worms depleted of ICD-2.
C) Representative "comma" embryo displaying button-like corpses indicative of apoptosis (arrows). **D)** Representative "normal" embryo displaying normal morphology, in this case three-fold stage, just prior to hatching. **E)** Representative "abnormal" embryo displaying abnormal morphology, in particular, disruption of the smooth, worm-like structure associated with this stage of development. **F)** Representative "pre-comma vacuolated" embryo displaying a large vacuolated region consistent with the death of epidermal or muscle cells early in development.

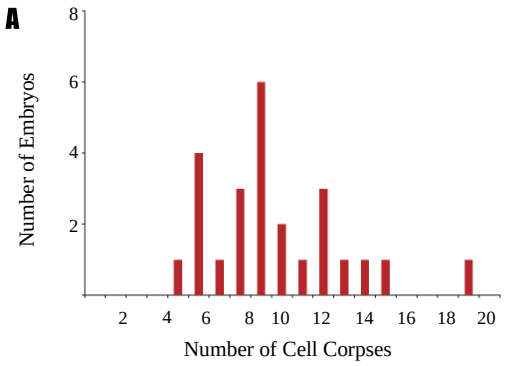
A
Number of Embryos
8
6
4
2
2 4 6 8 10 12 14 16 18 20
Number of Cell Corpses

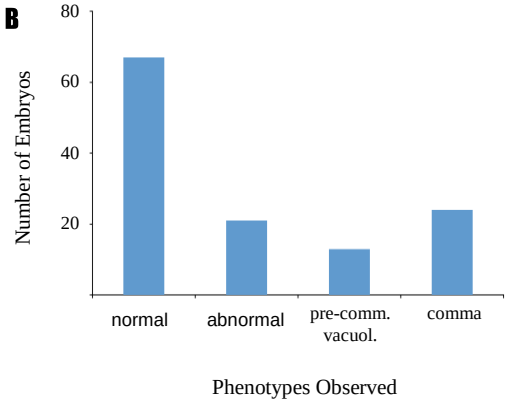
B
Number of Embryos
80
60
40
20
normal
abnormal
pre-comm. vacuol.
comma
Phenotypes Observed

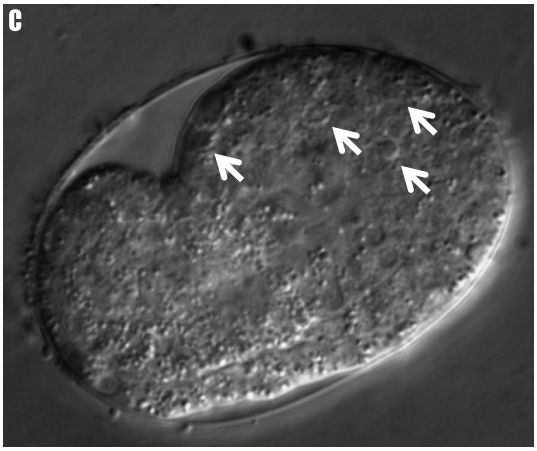
C


D

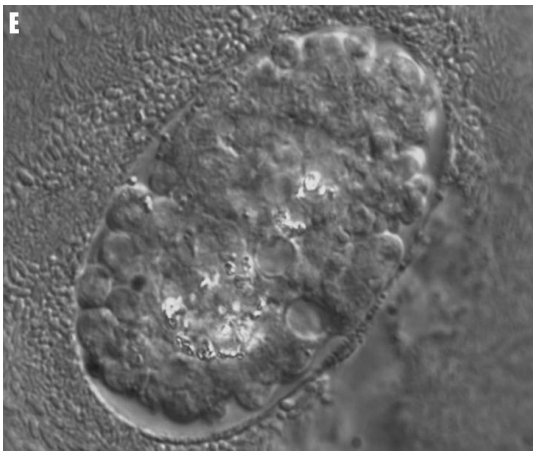
E

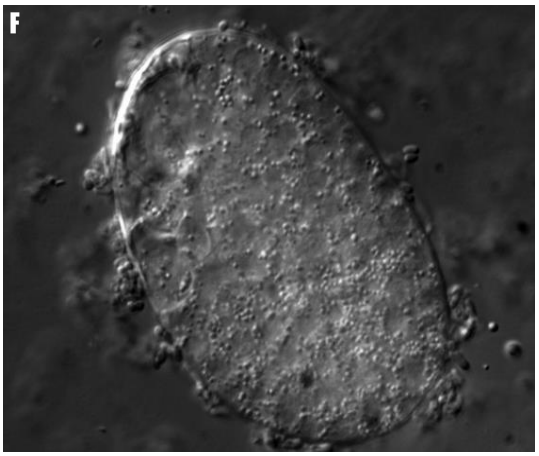
F

Figure 6. UPR effects in *ire-1*(ko) embryos depleted of ICD-2 at 1M IPTG. *ire-1*(ko) animals were treated with 1M IPTG-induced icd-2(RNAi) and their progeny characterized for effects on embryonic apoptosis and morphological development. **A)** Quantification of apoptotic cell corpses in *ire-1*(ko) embryos depleted of ICD-2 (n=33). Progeny of ICD-2-depleted worms were scored for the number of corpses assessed at comma stage of embryogenesis (~300 minutes post fertilization). **B)**Quantification of embryonic outcomes in *ire-1*(ko) embryos depleted of ICD-2 (n=228). Embryos were scored as "normal if they progressed past comma stage displaying normal morphology, as seen in D); embryos were scored as "abnormal" if they progressed past comma stage and displayed mutant morphology, as seen in E); embryos were scored as "pre-comma vacuolated" if they arrested prior to comma stage and contained regions of vacuolization, as seen in F); embryos were considered "comma" if they were scored at this stage and displayed wild type morphology, as seen in C). **C-F)** Representative progeny embryos from *ire*-(ko) adult worms depleted of ICD-2.
C) Representative "comma" embryo displaying button-like corpses indicative of apoptosis (arrows). **D)** Representative "normal" embryo displaying normal morphology, in this case three-fold stage, just prior to hatching. **E)** Representative "abnormal" embryo displaying abnormal morphology, in particular, disruption of the smooth, worm-like structure associated with this stage of development. **F)** Representative "pre-comma vacuolated" embryo displaying a large vacuolated region consistent with the death of epidermal or muscle cells early in development.

4.2 DEPLETION OF ICD-1 or ICD-2 in XBP-1 KNOCK OUT WORMS

The IRE-1 arm of the UPR bifurcates immediately downstream of the protein to activate two independent pathways; one pathway generates an active form of the transcription factor XBP-1, while the other pathway engages Jun kinase, which in turn initiates apoptosis. XBP-1 is thought to function soon after activation of IRE-1, and appears to control the expression of genes whose products have cell-saving functions, e.g. HSP-4. Activation of Jun kinase likely occurs as IRE-1 remains active in the face of prolonged stress, and is tasked with killing the cell that is unable to resolve misfolded protein levels effectively and efficiently. The previous experiments determined which stress-induced phenotypes generated by NAC depletion were dependent on IRE-1 function. To determine which phenotypes are dependent specifically on XBP-1, I performed NAC depletion assays in XBP-1 knockout animals, and measured the same set of stress-induced outputs.

4.2.1 APOPTOSIS IN XBP-1 KNOCKOUT WORMS DEPLETED OF ICD-1 OR ICD-2

To determine the effects of NAC depletion on embryonic apoptosis in embryos lacking XBP-1, I performed icd-1 or icd-2(RNAi) depletion experiments in XBP-1 knockout animals and quantified apoptosis at comma stage of development. Of the 369 XBP-1 knock out embryos depleted of ICD-1 observed, 81 comma stage embryos had an average corpse number of 11.09 (Standard deviation ± 3.56) and ranged from 1 corpse to 20 corpses (Figure 8a). Of the 554 XBP-1 knock out embryos depleted of ICD-2 observed, 108 comma stage embryos had an average corpse number of 10.27 (Standard deviation ± 2.57) and ranged from 4 to 22 corpses (Figure 9a). Both populations showed a statistically significant increase in the number of apoptotic corpses relative to untreated

XBP-1 knock out embryos (Average= 7.06, Standard Deviation ± 2.63, t-test $p<0.01$)(Figure 3), but were not significantly different from each other. Cell corpses were wild type in morphology and location in both populations (Figures 8 and 9). Of note, both ICD-1 and ICD-2-depleted populations in these experiments displayed higher levels of apoptosis than those seen in IRE-1 knockout embryos depleted of ICD-1 or ICD-2.

4.2.2 MORPHOLOGICAL DEFECTS IN XBP-1 KNOCKOUT WORMS DEPLETED OF ICD-1 OR ICD-2

As with IRE-1 knockout embryos, depletion of the NAC resulted in severely defective XBP-1 knockout embryos, but the percentage of abnormal embryos in these populations were increased relative to IRE-1 knockout populations. Both ICD-1 and ICD-2 depletion resulted in a relatively high percentage of morphologically abnormal embryos, ranging from 16-17% of the total population, as compared to a range of 21-36% in IRE-1 knockout populations depleted of the NAC. The most severely affected embryos exhibited morphological deformations such as large rounded protrusions and disrupted development (Figure 8e and 9e), similar to what was observed in IRE-1 experiments However, unlike IRE-1 mutant embryos, the late stage XBP-1 abnormal embryos had disorganized but recognizable structures (pharynx and gut), though the outer membranes were often disturbed.

4.2.3 EARLY EMBRYONIC LETHALITY IN XBP-1 KNOCK OUT WORMS DEPLTED OF ICD-1 OR ICD-2

As with the IRE-1 knockout animals, embryos produced by XBP-1 knockout worms depleted of ICD-1 or ICD-2 were observed for early embryonic lethality. Interestingly, while the percentage of abnormal embryos increased in XBP-1 knockouts

relative to IRE-1 knockouts, the percentage of embryos within this population that were early embryonic lethal decreased. Both ICD-1 and ICD-2 depleted abnormal populations showed a 4% rate of embryonic lethality compared with rates ranging from 10-14% in abnormal IRE1 embryos. As with IRE-1, though, XBP-1 abnormal embryos that arrested early also displayed large vacuolated spaces in the anterior region of the embryo (Figure 8F and 9F).

4.2.4 PRESENCE OF LYSOSOME IN XBP-1 KNOCK OUT WORMS DEPLETED OF ICD-1 OR ICD-2

With regards to XBP-1 knock out embryos depleted of ICD-1 or ICD-2, an increase in the general number and size of gut cell lysosomes was observed in severely defective embryos, similar to the effects seen in IRE-1 knockout embryos, with no discernible difference with regards to the subunit depleted. This effect, however, was less robust in XBP-1 mutants relative to IRE-1 mutants, and unlike IRE-1, no lysosomes were observed in comma stage embryos or earlier.

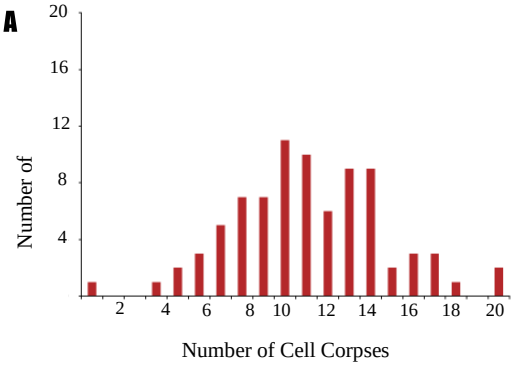
A
20
16
12
8
4
Number of
2
4
6
8
10
12
14
16
18
20
Number of Cell Corpses

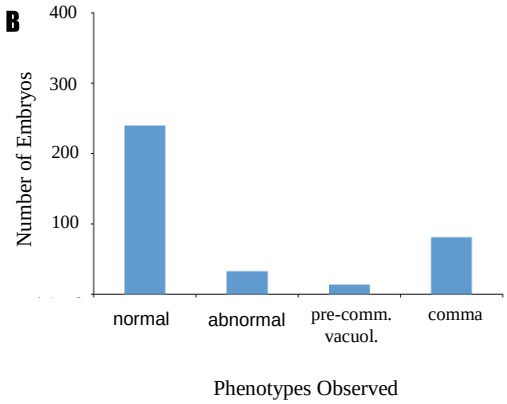
B
400
300
200
100
Number of Embryos
normal
abnormal
pre-comm.
vacuol.
comma
Phenotypes Observed

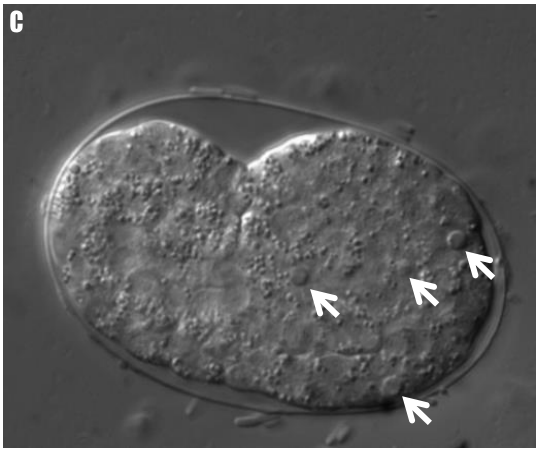
C


D

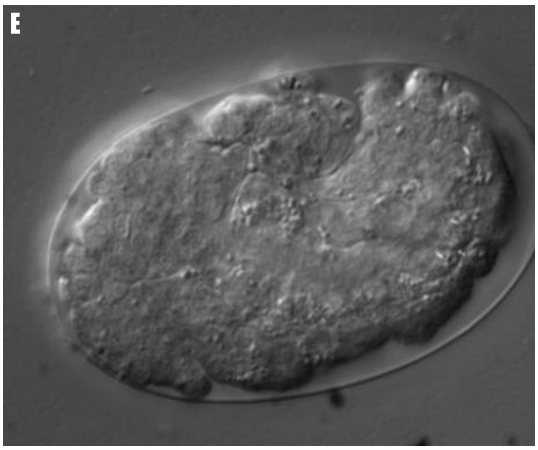
E

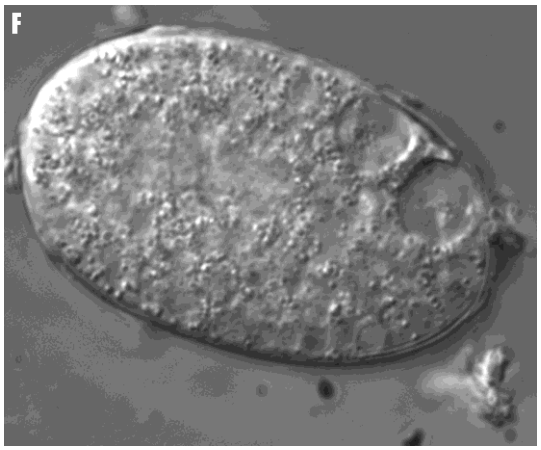
F

Figure 7. UPR effects in *xbp-1*(ko) embryos depleted of ICD-1. *xbp-1*(ko) animals were treated with *icd-1*(RNAi) and their progeny characterized for effects on embryonic apoptosis and morphological development. **A)** Quantification of apoptotic cell corpses in *xbp-1*(ko) embryos depleted of ICD-1 (n=81). Progeny of ICD-1-depleted worms were scored for the number of corpses assessed at comma stage of embryogenesis (~300 minutes post fertilization). **B)** Quantification of embryonic outcomes in *xbp-1*(ko) embryos depleted of ICD-1 (n=369). Embryos were scored as "normal" if they progressed past comma stage displaying normal morphology, as seen in D); embryos were scored as "abnormal" if they progressed past comma stage and displayed mutant morphology, as seen in E); embryos were scored as "pre-comma vacuolated" if they arrested prior to comma stage and contained regions of vacuolization, as seen in F); embryos were considered "comma" if they were scored at this stage and displayed wild type morphology, as seen in C).**C-F)** Representative progeny embryos from *xbp-1*(ko) adult worms depleted of ICD-1. **C)** Representative "comma" embryo displaying button-like corpses indicative of apoptosis (arrows). **D)** Representative "normal" embryo displaying normal morphology, in this case three-fold stage, just prior to hatching. **E)** Representative "abnormal" embryo displaying abnormal morphology, in particular, disruption of the smooth, worm-like structure associated with this stage of development. **F)** Representative "pre-comma vacuolated" embryo displaying a large vacuolated region consistent with the death of epidermal or muscle cells early in development.

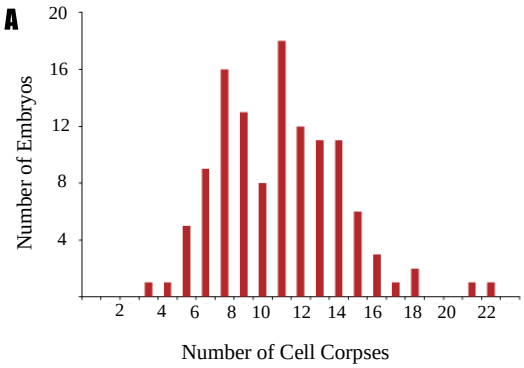
A
Number of Embryos
20
16
12
8
4
2 4 6 8 10 12 14 16 18 20 22
Number of Cell Corpses

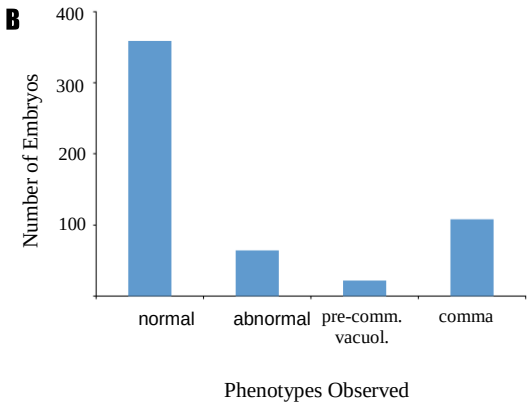
B
Number of Embryos
400
300
200
100
normal
abnormal
pre-comm. vacuol.
comma
Phenotypes Observed

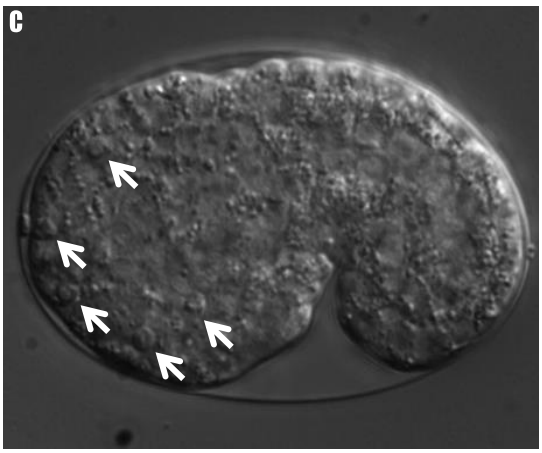
C

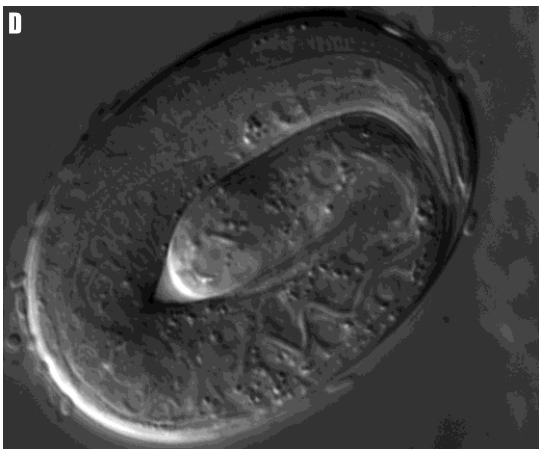
D

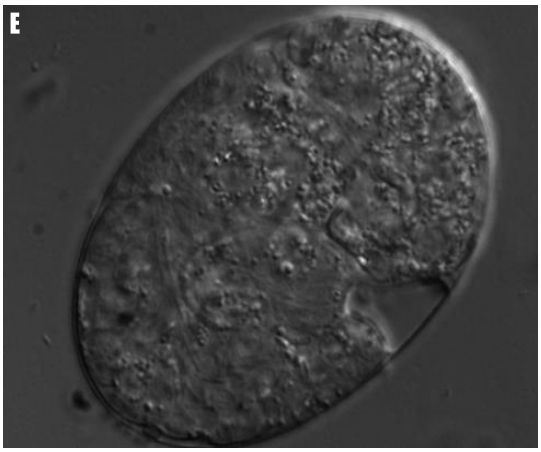
E

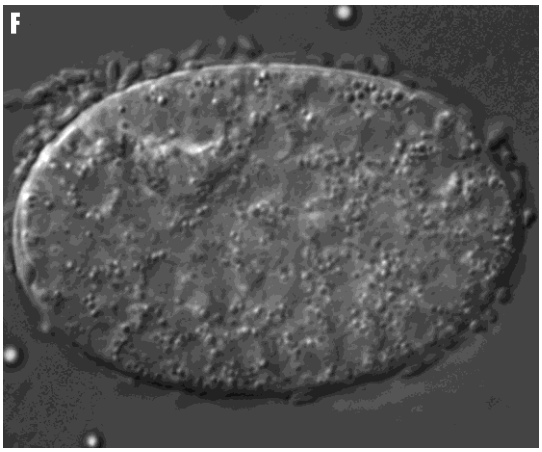
F

Figure 8. UPR effects in *xbp-1*(ko) embryos depleted of ICD-2. *xbp-1*(ko) animals were treated with icd-2(RNAi) and their progeny characterized for effects on embryonic apoptosis and morphological development. **A)** Quantification of apoptotic cell corpses in *xbp-1*(ko) embryos depleted of ICD-2 (n=108). Progeny of ICD-1-depleted worms were scored for the number of corpses assessed at comma stage of embryogenesis (~300 minutes post fertilization). **B)** Quantification of embryonic outcomes in *xbp-1*(ko) embryos depleted of ICD-2 (n=554). Embryos were scored as "normal" if they progressed past comma stage displaying normal morphology, as seen in D); embryos were scored as "abnormal" if they progressed past comma stage and displayed mutant morphology, as seen in E); embryos were scored as "pre-comma vacuolated" if they arrested prior to comma stage and contained regions of vacuolization, as seen in F); embryos were considered "comma" if they were scored at this stage and displayed wild type morphology, as seen in C). **C-F)** Representative progeny embryos from *xbp-1*(ko) adult worms depleted of ICD-2. **C)** Representative "comma" embryo displaying button-like corpses indicative of apoptosis (arrows). **D)** Representative "normal" embryo displaying normal morphology, in this case three-fold stage, just prior to hatching. **E)** Representative "abnormal" embryo displaying abnormal morphology, in particular, disruption of the smooth, worm-like structure associated with this stage of development. **F)** Representative "pre-comma vacuolated" embryo displaying a large vacuolated region consistent with the death of epidermal or muscle cells early in development.

4.3 DEPLETION OF ICD-1 OR ICD-2 IN PERK AND ATF6 KNOCK OUT WORMS

In *C. elegans* as well as other organisms, IRE-1 is known to be the primary contributor to the UPR during misfolded protein stress in the ER. It is therefore essential to understand the relationship between IRE-1 and the NAC during stress, but a complete picture of the UPR/NAC relationship requires assessment of the contributions the other two arms of the UPR make to the management of stress induced by NAC depletion. To this end, I performed ICD-1 and ICD-2 depletion assays on both PERK/PEK-1 knockout and ATF6 knockout animals, and evaluated the same stress-induced phenotypes as were assessed in IRE-1 and XBP-1 knockouts.

4.3.1 APOPTOSIS IN PERK/PEK-1 AND ATF6 KNOCKOUT WORMS DEPLETED OF ICD-1 OR ICD-2

As before, ICD-1 or -2 was depleted in PERK and ATF6 knockout animals, and comma-stage apoptosis was quantified. 115 PERK knockout embryos depleted of ICD-1 had an average of 10.50 corpses per embryo, ranging from 1 corpse to 26 corpses(Figure 10a), while164 embryos depleted of ICD-2 had an average number of cell corpses of 10.42 (Standard deviation ± 4.69) and ranged from 3 to 34 corpses (Figure 10a). (Standard deviation± 4.48) (Figure 11a). Both populations showed a statistically significant increase in the number of apoptotic corpses relative to untreated PERK knock out embryos.(Average=6.56, Standard Deviation ± 2.53, t-test ($p<0.01$))(Figure 3). 75 ATF6 knockout embryos depleted of ICD-1 had an average number of 11.22 corpses per embryo (standard deviation ± 4.66) and ranged from 4 to 21 corpses, while 79 ICD-2-depleted embryos averaged 9.94 corpses per embryo (Standard deviation ±3.44) and ranged from 3 to 20 corpses (Figure 12a). Both populations showed statistically significant increases relative to the untreated control, but were not statistically different

from each other. In all cases, the levels of apoptosis at comma stage upon depletion of the NAC are reminiscent of those observed in XBP-1 knockouts but not IRE-1 knockouts.

4.3.2 MORPHOLOGICAL DEFECTS IN PERK/PEK-1 AND ATF6 KNOCK OUT WORMS DEPLETED OF ICD-1 OR ICD-2

With regards to the morphological defects associated with depletion of ICD-1 or -2 in abnormal PERK and ATF6 embryos , both showed a subpopulation of defective embryos, but the percentages of these populations differed relative to each other. For PERK knockouts, depletion of ICD-1 or -2 resulted in an abnormal population in the range of 77-78% of the total population, while ATF6 percentages were appreciably lower at 64-66% (Figure 5). In addition to these quantitative differences, the mutant morphologies of these populations were also qualitatively different. The PERK abnormal population displayed a range of embryonic stages from mid- to late development that showed somewhat discernible internal structures, but still generally disorganized and misshapen. Abnormal ATF6 embryos, on the other hand, were generally able to progress late into embryonic development, with easily discernible internal structures and a well-formed body, save a consistently appearing protrusion at the anterior of the embryo (Figures 12, 13 and 5).

4.3.3 EARLY EMBRYONIC LETHALITY IN PERK/PEK-1 AND ATF6 KNOCK OUT WORMS DEPLETED OF ICD-1 OR ICD-2

In addition to the morphological differences observed between PERK and ATF6 upon NAC depletion, there was also a significant difference in the levels of early embryonic lethality observed between these populations. PERK knockout worms depleted of ICD-1 or -2 displayed an embryonic lethality rate ranging from 4-6%, with these embryos showing the same anterior vacuolization seen in IRE-1 and XBP-1 early

arresters depleted of the NAC (Figure 5). In addition, ATF6 knockouts depleted of ICD-2 showed an embryonic lethality rate of 3% with anterior vacuolization (Figures 5 and 13F). But, surprisingly, ATF6 knockouts depleted of ICD-1 showed no discernible embryonic lethality or any embryos with anterior vacuolization (Figure 12), the first evidence of differential effects on stress response in a UPR mutant dependent on which subunit is depleted.

4.3.4 PRESENCE OF LYSOSOMES IN PERK/PEK-1 AND ATF6 KNOCK OUT WORMS DEPLETED OF ICD-1 AND ICD-2

With regards to both PERK and ATF6 knock out embryos depleted of ICD-1 or ICD-2, the increase in the number and size of gut cell lysosomes seems comparable to the effect seen in abnormal XBP-1 embryos, but not abnormal IRE1 embryos qualitatively but requires further investigation and analysis. In all four cases, gut cell lysosomes were observed in a subset of late stage embryos (Figure 9e, 10e, 11e, 12e), but no lysosomes were observed in comma stage embryos or earlier.

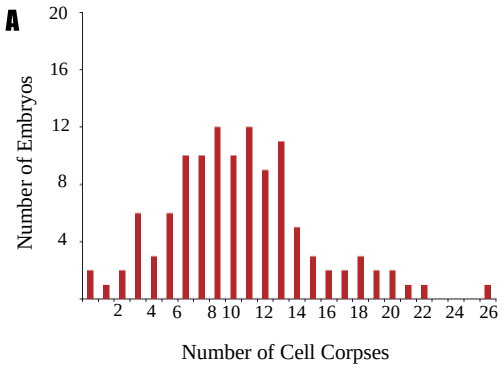
A
Number of Embryos
20
16
12
8
4
2 4 6 8 10 12 14 16 18 20 22 24 26
Number of Cell Corpses

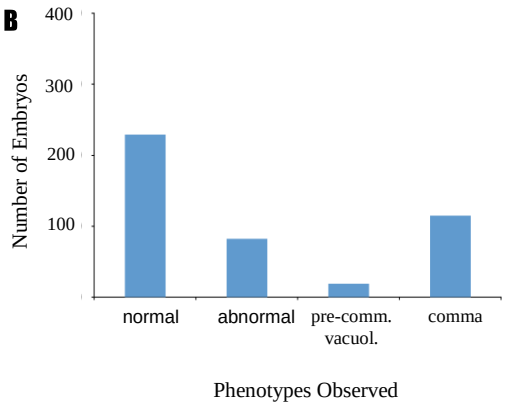
B
Number of Embryos
400
300
200
100
normal
abnormal
pre-comm. vacuol.
comma
Phenotypes Observed

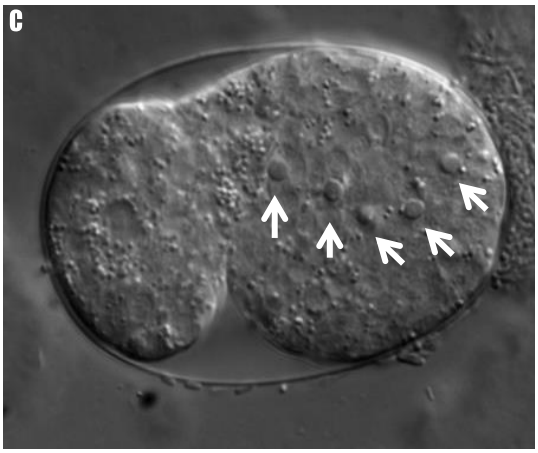
C

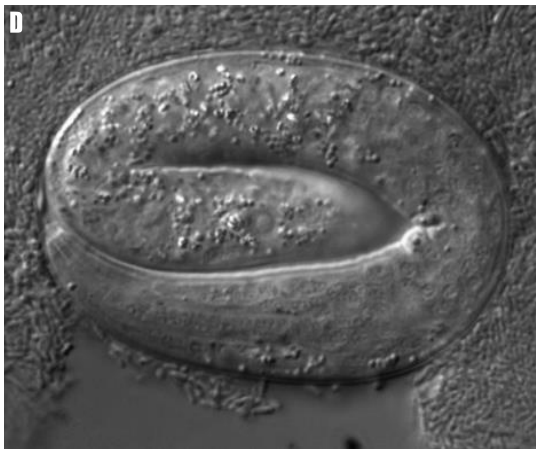
D

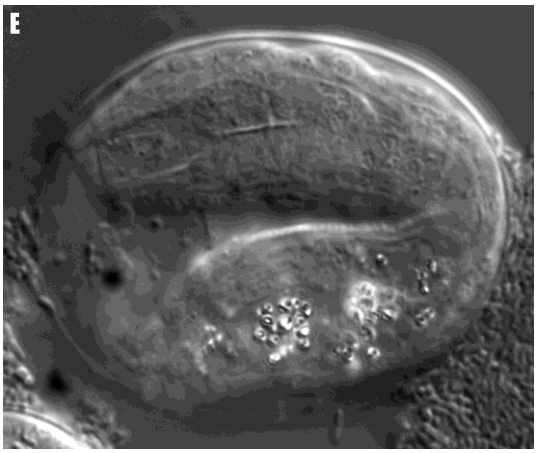
E

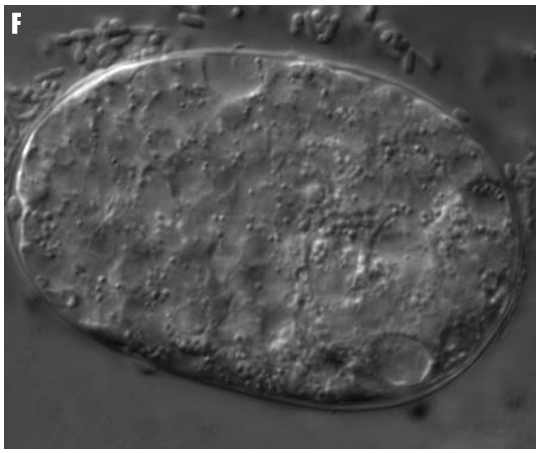
F

Figure 9. UPR effects in *pek-1*(ko) embryos depleted of ICD-1. *pek-1*(ko) animals were treated with icd-1(RNAi) and their progeny characterized for effects on embryonic apoptosis and morphological development. **A)** Quantification of apoptotic cell corpses in *pek-1*(ko) embryos depleted of ICD-2 (n=115). Progeny of ICD-1-depleted worms were scored for the number of corpses assessed at comma stage of embryogenesis (~300 minutes post fertilization). **B)** Quantification of embryonic outcomes in *pek-1*(ko) embryos depleted of ICD-2 (n=451). Embryos were scored as "normal" if they progressed past comma stage displaying normal morphology, as seen in D); embryos were scored as "abnormal" if they progressed past comma stage and displayed mutant morphology, as seen in E); embryos were scored as "pre-comma vacuolated" if they arrested prior to comma stage and contained regions of vacuolization, as seen in F); embryos were considered "comma" if they were scored at this stage and displayed wild type morphology, as seen in C).**C-F)** Representative progeny embryos from *pek-1*(ko) adult worms depleted of ICD-1. **C)** Representative "comma" embryo displaying button-like corpses indicative of apoptosis (arrows). **D)** Representative "normal" embryo displaying normal morphology, in this case three-fold stage, just prior to hatching. **E)** Representative "abnormal" embryo displaying abnormal morphology, in particular, disruption of the smooth, worm-like structure associated with this stage of development. **F)** Representative "pre-comma vacuolated" embryo displaying a large vacuolated region consistent with the death of epidermal or muscle cells early in development.

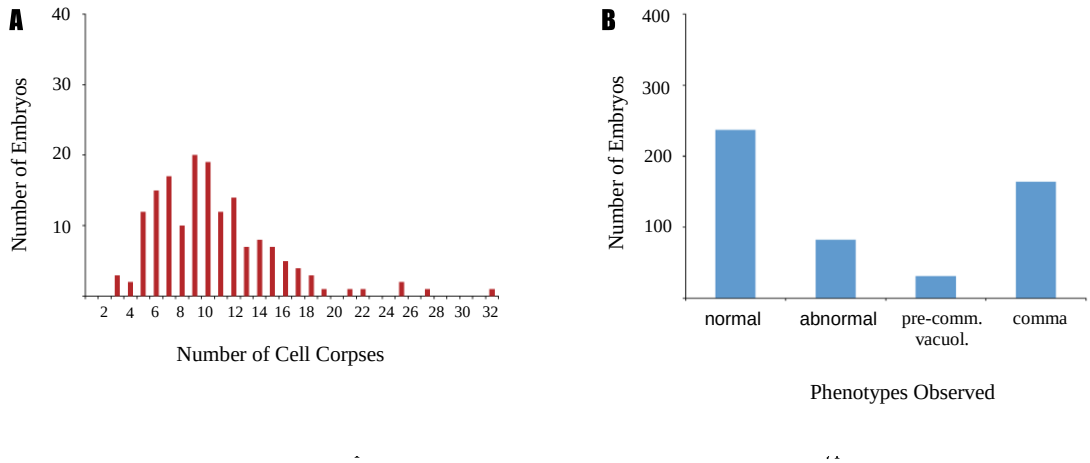
A
Number of Embryos
40
30
20
10
2 4 6 8 10 12 14 16 18 20 22 24 26 28 30 32
Number of Cell Corpses
B
Number of Embryos
400
300
200
100
normal
abnormal
pre-comm. vacuol.
comma
Phenotypes Observed

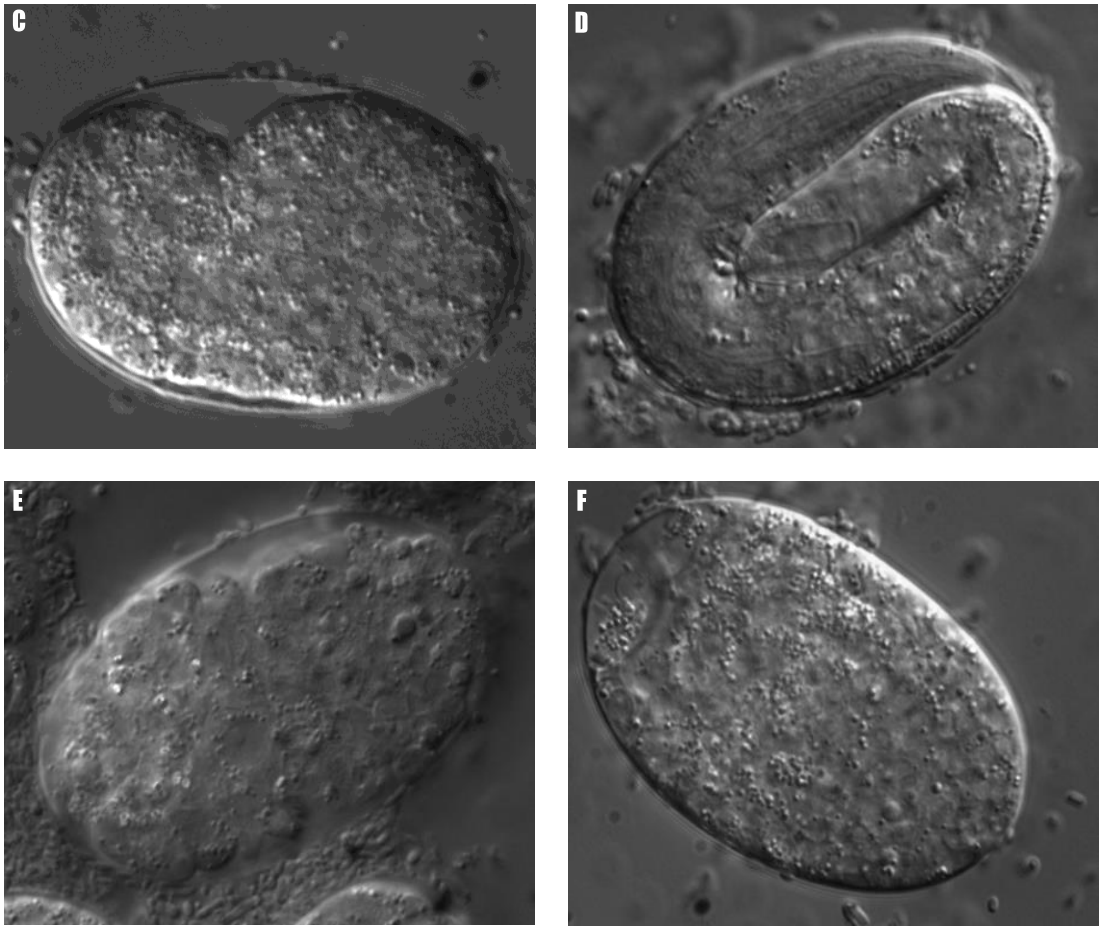
C
D
E
F

Figure 10. UPR effects in *pek-1*(ko) embryos depleted of ICD-2. *pek-1*(ko) animals were treated with icd-1(RNAi) and their progeny characterized for effects on embryonic apoptosis and morphological development. **A)** Quantification of apoptotic cell corpses in *pek-1*(ko) embryos depleted of ICD-1 (n=164). Progeny of ICD-2-depleted worms were scored for the number of corpses assessed at comma stage of embryogenesis (~300 minutes post fertilization). **B)** Quantification of embryonic outcomes in *pek-1*(ko) embryos depleted of ICD-2 (n=527). Embryos were scored as "normal" if they progressed past comma stage displaying normal morphology, as seen in D); embryos were scored as "abnormal" if they progressed past comma stage and displayed mutant morphology, as seen in E); embryos were scored as "pre-comma vacuolated" if they arrested prior to comma stage and contained regions of vacuolization, as seen in F); embryos were considered "comma" if they were scored at this stage and displayed wild type morphology, as seen in C). **C-F)** Representative progeny embryos from *pek-1*(ko) adult worms depleted of ICD-2. **C)** Representative "comma" embryo displaying button-like corpses indicative of apoptosis (arrows). **D)** Representative "normal" embryo displaying normal morphology, in this case three-fold stage, just prior to hatching. **E)** Representative "abnormal" embryo displaying abnormal morphology, in particular, disruption of the smooth, worm-like structure associated with this stage of development. **F)** Representative "pre-comma vacuolated" embryo displaying a large vacuolated region consistent with the death of epidermal or muscle cells early in development.

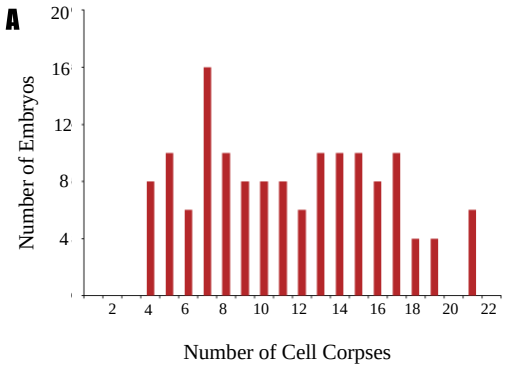
A
Number of Embryos
20
16
12
8
4
2
4
6
8
10
12
14
16
18
20
22
Number of Cell Corpses

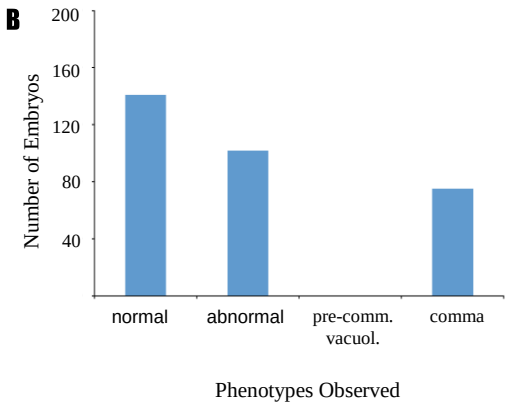
B
Number of Embryos
200
160
120
80
40
normal
abnormal
pre-comm. vacuol.
comma
Phenotypes Observed

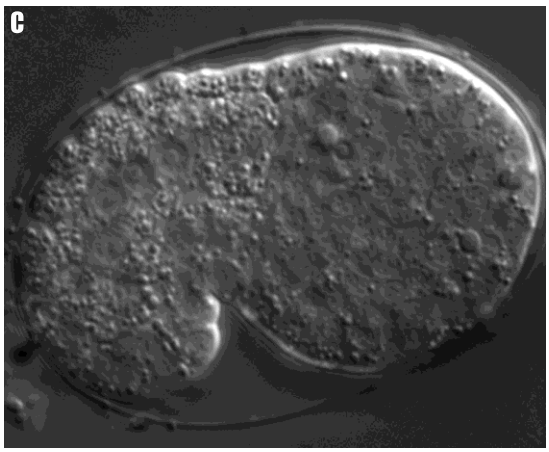
C


D

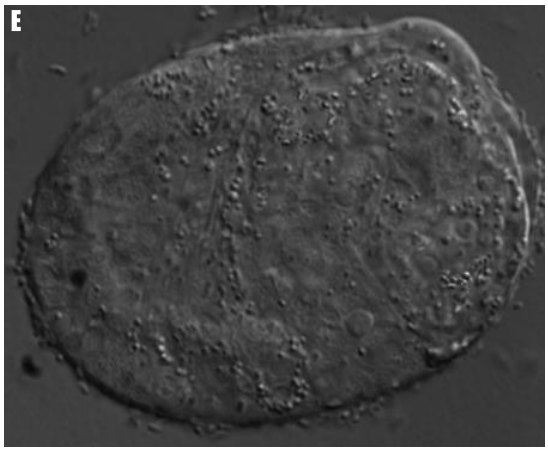
E

Figure 11. UPR effects in *atf6*(ko) embryos depleted of ICD-1. *atf6*(ko) animals were treated with *icd-1*(RNAi) and their progeny characterized for effects on embryonic apoptosis and morphological development. **A)** Quantification of apoptotic cell corpses in *atf6*(ko) embryos depleted of ICD-1 (n=75). Progeny of ICD-1-depleted worms were scored for the number of corpses assessed at comma stage of embryogenesis (~300 minutes post fertilization). **B)** Quantification of embryonic outcomes in *atf6*(ko) embryos depleted of ICD-1 (n=320). Embryos were scored as "normal" if they progressed past comma stage displaying normal morphology, as seen in D); embryos were scored as "abnormal" if they progressed past comma stage and displayed mutant morphology, as seen in E); embryos were scored as "pre-comma vacuolated" if they arrested prior to comma stage and contained regions of vacuolization, as seen in F); embryos were considered "comma" if they were scored at this stage and displayed wild type morphology, as seen in C). **C-E)** Representative progeny embryos from *atf6*(ko) adult worms depleted of ICD-1. **C)** Representative "comma" embryo displaying button-like corpses indicative of apoptosis (arrows). **D)** Representative "normal" embryo displaying normal morphology, in this case three-fold stage, just prior to hatching. **E)** Representative "abnormal" embryo displaying abnormal morphology, in particular, disruption of the smooth, worm-like structure associated with this stage of development.

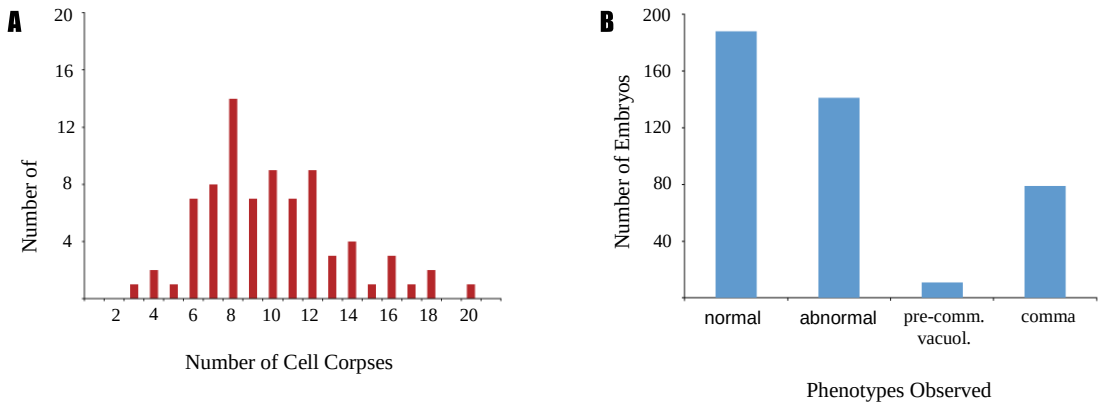
A
20
16
12
8
4
Number of
2 4 6 8 10 12 14 16 18 20
Number of Cell Corpses
B
200
160
120
80
40
Number of Embryos
normal
abnormal
pre-comm. vacuol.
comma
Phenotypes Observed

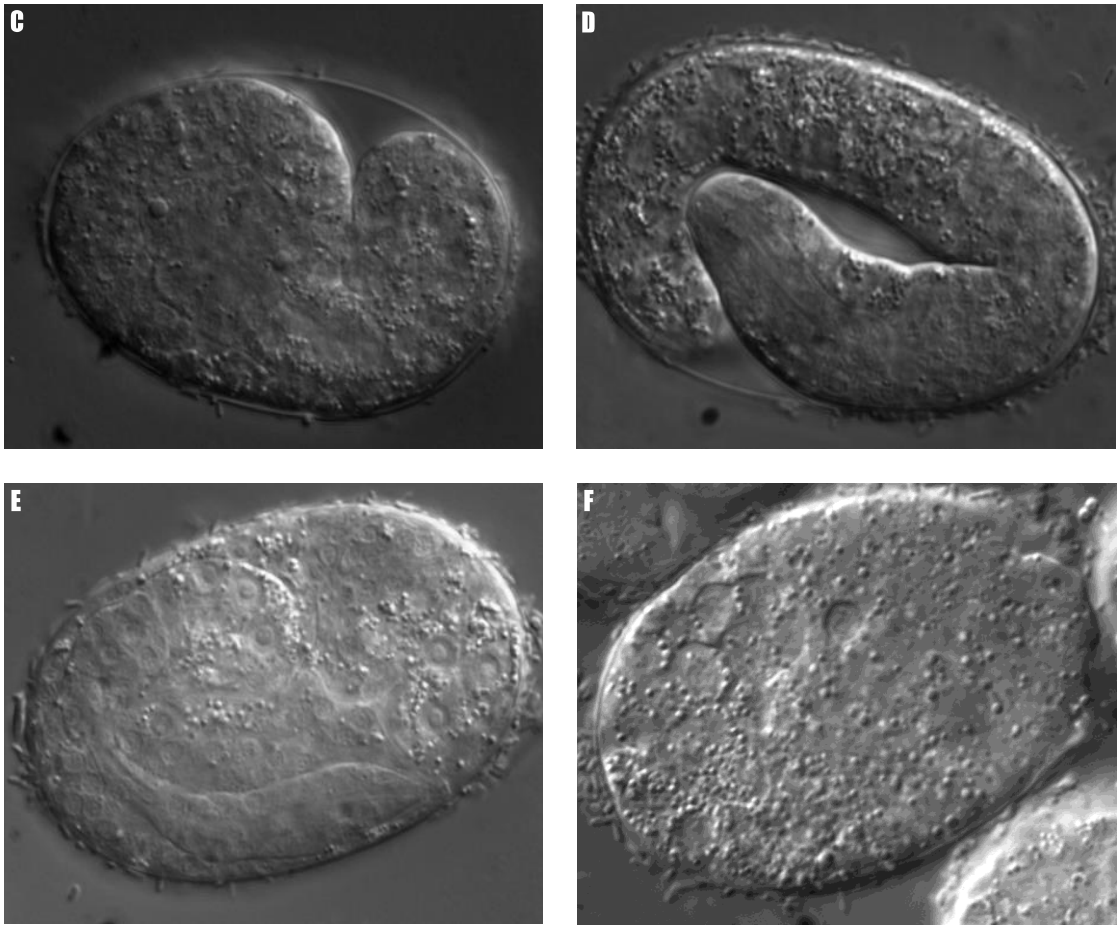
C
D
E
F

Figure 12. UPR effects in *atf6*(ko) embryos depleted of ICD-2. *atf6*(ko) animals were treated with icd-2(RNAi) and their progeny characterized for effects on embryonic apoptosis and morphological development. **A)** Quantification of apoptotic cell corpses in *atf6*(ko) embryos depleted of ICD-2 (n=79). Progeny of ICD-2-depleted worms were scored for the number of corpses assessed at comma stage of embryogenesis (~300 minutes post fertilization). **B)** Quantification of embryonic outcomes in *atf6*(ko) embryos depleted of ICD-2 (n=421). Embryos were scored as "normal if they progressed past comma stage displaying normal morphology, as seen in D); embryos were scored as "abnormal" if they progressed past comma stage and displayed mutant morphology, as seen in E); embryos were scored as "pre-comma vacuolated" if they arrested prior to comma stage and contained regions of vacuolization, as seen in F); embryos were considered "comma" if they were scored at this stage and displayed wild type morphology, as seen in C). **C-F)** Representative progeny embryos from *atf6*(ko) adult worms depleted of ICD-2. **C)** Representative "comma" embryo displaying button-like corpses indicative of apoptosis (arrows). **D)** Representative "normal" embryo displaying normal morphology, in this case three-fold stage, just prior to hatching. **E)** Representative "abnormal" embryo displaying abnormal morphology, in particular, disruption of the smooth, worm-like structure associated with this stage of development. **F)** Representative "pre-comma vacuolated" embryo displaying a large vacuolated region consistent with the death of epidermal or muscle cells early in development.

5. DISCUSSION

In a properly functioning cell, the role of a chaperone is to bind non-native proteins and aid in proper folding or refolding. Chaperones provide protection for nascent proteins as they exit the ribosome, prevent inappropriate interactions, aid in assembly of complex structures, and can be responsible for the recognition and resolution of misfolded proteins (Lodish et al., 2007). Under normal conditions, chaperones are essential for establishing the appropriate protein profile for a particular cell; during misfolded protein stress, chaperone expression levels and activities are directly linked to stress response mechanisms engaged to either save or eliminate the cell. As such, chaperones are positioned to be both sensors of levels of misfolded protein stress and active participants in the resulting response. To understand how cells manage misfolded protein stress, we have to first understand this interplay between chaperones and the other elements of stress response. e.g. the UPR, as the stress is first sensed and then mitigated. From this, we can gain a better understanding of how these interactions may be altered in the myriad diseases associated with abnormal protein folding.

One current model of NAC function putatively places it at the interface between misfolded protein stress and the subsequent response. The primary proposed function of the NAC is as translational chaperone. As such, the NAC aids in protein folding while shuttling these proteins during translation to compartments of the cell that are not the ER, thereby preventing their mislocalization to the ER (Rospert, Dubaquie, & Gautschi, 2002). These functions protect the cell from misfolded protein stress in two ways: by promoting proper folding during translation and also preventing the overloading of protein-folding systems in the ER. In the context of this model, the NAC's unique profile

within the chaperone family (functional as a two subunit complex, bound directly to the ribosome and requiring no ATP for its effects) in turn predicts a unique relationship of the NAC with the ER-specific UPR during misfolded protein stress in that organelle. Until recently, this relationship has gone largely unexplored, and is the focus of my studies.

While the translational chaperone model of NAC function has been proposed for a number of years, recent evidence is only now starting to support this model. The necessity of NAC for viability in vertebrate and invertebrate metazoans has been well established: knockouts of one or the other subunit in mice, *Drosophila melanogaster* and *C. elegans* all result in early embryonic lethality (Bloss et al., 2003; Deng & Behringer, 1995; Markesh et al., 2000). The importance of NAC function to cell survival is tempered, however, by the finding that deletion of either or both subunits has virtually no effect in yeast. Nevertheless, it was in yeast that a connection between NAC function and protein folding was first truly established; knockout of the NAC in conjunction with the elimination of the SSB-RAC chaperone system lead to an increase in both misfolded protein levels and lethality relative to the elimination of either system alone (Koplin et al., 2011). Subsequent work in *C. elegans* has shown that depletion of the NAC increases misfolded protein levels in adults, during which bound NAC is sequestered away from the ribosome and the βNAC/ ICD-1 subunit associates with misfolded protein. Once the stress has been resolved, the NAC complex re-associates with the ribosome, suggesting a direct link between the activity of the NAC and resolution of misfolded protein stress (Kiersten-Miles, 2013). NAC's relationship to specific stress responders in this context, though, is an area of active research, including my studies.

That NAC function is related to management of protein folding specifically in the ER was confirmed in *C. elegans,* where NAC-depletion resulted in the up-regulation of the ER-specific chaperone HSP-4/BiP. Increased levels of this chaperone directly implicate engagement of the UPR as well, in that specific UPR components drive *hsp-4* gene expression during stress (Arsenovic et al., 2012). To further elucidate the relationship of NAC with the UPR and the management of misfolded protein stress, I took a systematic approach of depleting ICD-1/βNAC or ICD-2/αNAC in different UPR-deficient animals to determine which elements of the UPR, if any, are responsible for three different stress-response phenotypes associated with loss of NAC function: an increase in apoptosis, an increase in morphological defects, and an increase in lysosomal number and size in intestinal cells. In the process, I begin to determine not only the components involved in generating these phenotypes, but also gained insights into how these UPR pathways may contribute to the manifestation of these phenotypes.

IRE1 is the most evolutionarily ancient arm of the UPR, being conserved from yeast to humans, so we were particularly interested in determining the putative contributions of IRE-1 to phenotypes induced by NAC depletion (Sidrauski, C., 1997). In response to misfolded protein stress in the ER, HSP-4 disassociates from IRE1, allowing for its oligomerization, and activation at the ER membrane (Bertolotti et al., 2000; Ma et al., 2002; Shen et al., 2002). Activated IRE1 is an endonuclease that splices the mRNA that codes for the transcription factor XBP-1, which is responsible for controlling the transcription of UPR-related genes (Cox, 1996., Mori, 1996., Yoshida, 2001., Calfon, 2002). Prolonged activation of IRE1 also leads to the activation of an alternative pathway that results in the activation of Jun kinase (JNK), responsible for the

activation of pro-apoptotic and pro-autophagic mechanisms (Ozcan et al., 2004, Gabai et al., 1998, Yoneda et al., 2001).

Our observations support the hypothesis that stress induced by the depletion of NAC activates IRE1 pathways in *C. elegans*. Specifically, depletion of either NAC subunit reduced worm viability, stunted development and resulted in sterility in *ire-1*(ko) animals, indicating the importance of IRE1 in maintaining viability and fertility in the presence of ER stress induced by NAC depletion. IRE1 knockout embryos with sub-optimal depletion of the NAC surprisingly resulted in the induction of some UPR phenotypes but not others. Most interestingly, there was no significant increase in apoptosis in NAC depleted populations relative to the untreated IRE1(ko) control. This result is particularly noteworthy, in that *ire-1*(ko) embryos were the only UPR mutants that did not display an increase apoptosis when NAC was depleted, likely due to the loss of JNK-mediated apoptotic pathways normally induced by IRE1 activation. While IRE-1 is not the only activator of JNK, it appears to be the major modulator of JNK-initiated apoptosis as a result of ER stress. Consistent with this result, NAC depletion in XBP-1(ko) embryos, which retain the JNK-specific pathway of IRE-1, displayed an increase in apoptosis comparable to levels seen in other UPR mutants as well as wild type embryos. In light of these results, it is likely that the increase in apoptosis associated with NAC depletion to the activation of the JNK via IRE-1.

While the increase in apoptosis associated with NAC depletion appears to be dependent on the presence of IRE-1, phenotypic markers (e.g.the presence of birefringent lysosomes) associated with stress-induced autophagy were not suppressed in either NAC depleted *ire-1*(ko) or *xbp-1*(ko) populations, possibly indicating that other

arms of the UPR may contribute to this stress-induced phenotype. In addition, the increase in number and size of these birefringent lysosomal structures was only detectible in gut cells, possibly indicating cell specific stress responses to the depletion of the NAC. During UPR, the stress induced in the ER may overload already present protein turnover mechanisms, and require alternative disposal pathways such as the lysosomes generated by autophagy. Since this increase in the number and size of the lysosomes appears to be restricted to gut cells, bias towards the apoptosis seen primarily in neurons versus the autophagy observed in gut cells is further indication of cell-specific UPR activity in response to NAC depletion. *ire-1*(ko) and *xbp-1*(ko) embryos depleted of either *icd-1* or *icd-2* were scored for embryonic morphology, and a similar proportion of mutant and wild type embryos was observed in both cases. Affected embryos exhibited similar lumpy protrusions consistent with enclosure defects. *ire-1*(ko) worms, in particular, were slow to develop and move, small, and distended in shape, reminiscent of a "dumpy" phenotype observed in worms with defective cuticle formation. Both the enclosure defects and the dumpy phenotype are thought to result from defects in epidermal cell function, and may indicate that IRE-1 is necessary to prevent loss of, or damage to, epidermal cells in the face of stress induced by depletion of the NAC.

The possible loss of epidermal cells in *ire-1*(ko) embryos depleted of the NAC, with no concurrent evidence of apoptosis in these regions of the embryo, may indicate that this stress has the potential to disrupt cell differentiation patterns in the absence of IRE-1 activity. In all NAC-depleted IRE1 populations, a higher proportion of embryos arrested around 80-cell stage, and vacuolization was consistently observed in a sickle shape towards the anterior of the embryo in an area mapped to produce either muscle or

epidermal cells. Vacuolization, as opposed to the corpses generated during apoptosis, results from necrosis, which itself may be the result of a failed differentiation program in these cells. Induction of differentiation in many cell types appears to be dependent on the UPR, and secretory cells in particular seem to rely on the UPR for differentiation, likely due to their need for tight control of protein folding and processing in the ER. Similar cessation of growth early in embryogenesis has been observed in IRE1 knockout *D. melanogaster* and mice, also perhaps due, at least in part, to differentiation defects (Reimold et al., 2000; Zhang et al., 2005). Due to the fact that IRE1 is the most evolutionarily ancient arm of the UPR, it is possible IRE-1's original role in the cell was as a facilitator of secretory cell differentiation, and that its association with ER protein homoestasis in this context allowed it to evolve into a manager of misfolded protein stress in all cells. *xbp-1*(ko) treatments yielded similar vacuolization phenotypes in a smaller proportion of affected embryos, indicating that the XBP-1 arm of IRE-1 may contribute to cell differentiation in times of stress, but may not be the only IRE-1-specific contributor.

Unlike the early embryonic arrest observed in *ire1*(ko) embryos depleted of the NAC, depletion of the NAC in *pek-1*(ko) embryos resulted in abnormal embryos that reached mid- to late development, and were able to form discernable, though misshapen, structures, indicating that loss of PEK-1 in the presence of NAC depletion is less traumatic to embryogenesis than the loss of IRE-1. Also, a small proportion of embryos exhibited early vacuolization, indicating that removal of PEK-1 may play a less significant role in cell differentiation and that it may be partially redundant with other UPR elements (Figure 3).

Depletion of the NAC in *pek-1*(ko) embryos resulted in a large increase in apoptosis relative to untreated *pek-1*(ko) embryos, consistent with the interpretation that PEK-1 activity during stress saves a number of cells that would be otherwise killed. Since one important role of PEK-1 is to attenuate translation of mRNAs, disruption of its function likely stunts the ability of the UPR to mitigate stress in the ER (Bertolotti, 2000). The continual influx of protein into the ER in the absence of PEK-1 may lead to stress that is sometimes short-lived but has the potential to become chronic, increasing the likelihood of apoptosis in the affected cell. The presence of IRE1 in these mutants likely facilitates the initiation of apoptosis, as the JNK apoptotic pathways remain intact.

As with abnormal IRE1 embryos, an increase in lysosomal size was observed in *pek-1*(ko) embryos depleted of the NAC, indicating that presence of functional PEK-1 may not be required for this autophagic response. Also similar to IRE1 (ko) results, the lysosomes were observed in the gut cells of the embryos, adding support to the concept that UPR activity in the face of misfolded protein stress tilts towards apoptosis or autophagy, depending on the cell type. Quantitative comparisions between lysosomes of these treatment groups is necessary to further support these observations.

Depletion of the NAC in *atf-6*(ko) worms produced, in general, milder versions of the stress-induced phenotypes seen in *ire-1*(ko) and *pek-1*(ko) embryos, indicating that loss of ATF-6 function is less detrimental to embryos undergoing misfolded protein stress relative to the loss of either IRE-1 or PEK-1. As with these other two arms of the UPR, *atf-6* (ko) populations displayed a relatively high percentage of mutant embryos (Figure 5) but most were later stage embryos with easily discernable internal structures and a well formed body save for a consistent protrusion from the anterior of many embryos; in other

words, they were the most well-developed abnormal embryos of any experimental population. In addition, the vacuolization seen in both *ire-1*(ko) and *pek-1*(ko) early embryos is largely absent in *atf-6*(ko) embryos, again indicating that the stress responses generated upon depletion of the NAC seem to rely little on the activity of ATF-6. Interestingly, a small proportion of *atf-6*(ko) depleted of ICD-2/αNAC did display early embryonic vacuolization while no early embryonic vacuolization was observed in *atf-6*(ko) worms depleted of ICD-1/βNAC, marking the first time I observed a difference in phenotypes relative to the NAC subunit depleted. The significance of this possibility remains to be investigated.

While ATF-6 appears to be the least important contributor to the UPR in the absence of the NAC, lysosomal increases in size were comparable to those seen in the other abnormal embryos, indicating that misfolded protein stress is still occurring in these embryos. Due to the presence of both functioning pro-autophagic and pro-apoptotic arms of the UPR (PERK and IRE1), the presence of lysosomes in *atf-6*(ko) embryos was not surprising, and may indicate the UPR is compromised at some level by the removal of AFT6.

With the exception of pre-comma vacuolated embryos seen in ATF-6 (ko) treatments, there was no noticeable difference in phenotypes observed within a abnormal population whether ICD-1 or ICD-2 was depleted. This result is surprising in light of evidence that both subunits appear to function apart from each other, either as monomers or homodimers. One interpretation of these results is that the stress-induced phenotypes we chose to assess are the result of the loss of NAC function alone, as opposed to the result of activities each subunit might perform in the absence of the other subunit. Further

analysis of the NAC/UPR relationship may identify more subtle phenotypes dependent on ICD-1 or ICD-2 activity in the absence of its binding partner.

In conclusion, our findings suggest that removal of either NAC subunit is enough to produce a misfolded protein stress in the ER and a subsequent UPR, and the phenotypic outcomes of this stress vary when specific UPR components are removed. This comprehensive analysis of the relationship of the UPR to the activities of the NAC has produced many varied and interesting results, but several important points fall out. One is that loss of IRE-1 has the most dramatic effect on UPR management of the stress induced by depletion of the NAC, both at the level of initiation of stress-induced apoptosis and at the level of embryonic development during this stress. For the first time since apoptosis was originally identified as a hallmark response to NAC depletion over tens year ago, I can at least in part ascribe this apoptotic response to the JNK arm of the IRE-1 pathway. In addition, we now know that IRE-1 activity during stress appears essential for early embryonic development in *C. elegans*, consistent with observations made in Drosophila and mice. We also know that PEK-1 appears to delay the initiation of apoptosis in cells depleted of the NAC, likely through its ability to attenuate translation, while ATF-6 appears to play a minor role UPR activity related to depletion of the NAC. In addition, the generation of numerous large lysosomes in the gut cells of all UPR mutants reflects that this stress response is either completely independent of the UPR or, more likely, generated through redundant UPR activities.

The results and the interpretation of these studies may provide important insights into the pathologies of human disease. There are a number of examples of neurodegenerative diseases that show either reduced levels of NAC subunits or reduced

activity of the UPR. In some cases, the disease displays both, as with Alzheimer's, where affected neurons display both reduced expression of αNAC and reduced IRE-1 activity. If we are to understand any potential disruption of interactions between the NAC and the UPR that could lead to disease, we first need to define the nature of these interactions. As such, the analyses presented above are steps in the right direction, and provide the foundation for further studies of this important issue.

6. REFERENCES

Arsenovic, P. T., Maldonado, A. T., Colleluori, V. D., & Bloss, T. A. (2012). Depletion of the C. elegans NAC engages the unfolded protein response, resulting in increased chaperone expression and apoptosis. *PLoS One, 7*(9), e44038. doi: 10.1371/journal.pone.0044038

Bertolotti, A., Zhang, Y., Hendershot, L. M., Harding, H. P., & Ron, D. (2000). Dynamic interaction of BiP and ER stress transducers in the unfolded-protein response. *Nat Cell Biol, 2*(6), 326-332. doi: 10.1038/35014014

Bloss, T. A., Witze, E. S., & Rothman, J. H. (2003). Suppression of CED-3-independent apoptosis by mitochondrial betaNAC in Caenorhabditis elegans. *Nature, 424*(6952), 1066-1071. doi: 10.1038/nature01920

Brandt, F., Etchells, S. A., Ortiz, J. O., Elcock, A. H., Hartl, F. U., & Baumeister, W. (2009). The native 3D organization of bacterial polysomes. *Cell, 136*(2), 261-271. doi: 10.1016/j.cell.2008.11.016

Calfon, M., Zeng, H., Urano, F., Till, J. H., Hubbard, S. R., Harding, H. P., . . . Ron, D. (2002). IRE1 couples endoplasmic reticulum load to secretory capacity by processing the XBP-1 mRNA. *Nature, 415*(6867), 92-96. doi: 10.1038/415092a

Caplan, A. J., Cyr, D. M., & Douglas, M. G. (1993). Eukaryotic homologues of Escherichia coli dnaJ: a diverse protein family that functions with hsp70 stress proteins. *Mol Biol Cell, 4*(6), 555-563.

Coelho, D. S., Cairrao, F., Zeng, X., Pires, E., Coelho, A. V., Ron, D., . . . Domingos, P. M. (2013). Xbp1-independent Ire1 signaling is required for photoreceptor

differentiation and rhabdomere morphogenesis in Drosophila. *Cell Rep, 5*(3), 791-801. doi: 10.1016/j.celrep.2013.09.046

Conradt, B., & Xue, D. (2005). Programmed cell death. *WormBook,* 1-13. doi: 10.1895/wormbook.1.32.1

Cox, J. S., & Walter, P. (1996). A novel mechanism for regulating activity of a transcription factor that controls the unfolded protein response. *Cell, 87*(3), 391-404.

Cross, B. C., Bond, P. J., Sadowski, P. G., Jha, B. K., Zak, J., Goodman, J. M., . . . Harding, H. P. (2012). The molecular basis for selective inhibition of unconventional mRNA splicing by an IRE1-binding small molecule. *Proc Natl Acad Sci U S A, 109*(15), E869-878. doi: 10.1073/pnas.1115623109

del Alamo, M., Hogan, D. J., Pechmann, S., Albanese, V., Brown, P. O., & Frydman, J. (2011). Defining the specificity of cotranslationally acting chaperones by systematic analysis of mRNAs associated with ribosome-nascent chain complexes. *PLoS Biol, 9*(7), e1001100. doi: 10.1371/journal.pbio.1001100

Deng, J. M., & Behringer, R. R. (1995). An insertional mutation in the BTF3 transcription factor gene leads to an early postimplantation lethality in mice. *Transgenic Res, 4*(4), 264-269.

Dobson, C. M. (2003). Protein folding and misfolding. *Nature, 426*(6968), 884-890. doi: 10.1038/nature02261

Fink, A. L. (1999). Chaperone-mediated protein folding. *Physiol Rev, 79*(2), 425-449.

Gabai, V. L., Meriin, A. B., Yaglom, J. A., Volloch, V. Z., & Sherman, M. Y. (1998). Role of Hsp70 in regulation of stress-kinase JNK: implications in apoptosis and aging. *FEBS Lett, 438*(1-2), 1-4.

Georgopoulos, C., & Welch, W. J. (1993). Role of the major heat shock proteins as molecular chaperones. *Annu Rev Cell Biol, 9*, 601-634. doi: 10.1146/annurev.cb.09.110193.003125

Guo, F. J., Jiang, R., Li, X., Zhang, P., Han, X., & Liu, C. (2014). Regulation of chondrocyte differentiation by IRE1alpha depends on its enzymatic activity. *Cell Signal, 26*(9), 1998-2007. doi: 10.1016/j.cellsig.2014.05.008

Hartl, F. U. (1996). Molecular chaperones in cellular protein folding. *Nature, 381*(6583), 571-579. doi: 10.1038/381571a0

Haze, K., Yoshida, H., Yanagi, H., Yura, T., & Mori, K. (1999). Mammalian transcription factor ATF6 is synthesized as a transmembrane protein and activated by proteolysis in response to endoplasmic reticulum stress. *Mol Biol Cell, 10*(11), 3787-3799.

Hetz, C., Bernasconi, P., Fisher, J., Lee, A. H., Bassik, M. C., Antonsson, B., . . . Korsmeyer, S. J. (2006). Proapoptotic BAX and BAK modulate the unfolded protein response by a direct interaction with IRE1alpha. *Science, 312*(5773), 572-576. doi: 10.1126/science.1123480

Jellinger, K. A. (2009). Recent advances in our understanding of neurodegeneration. *J Neural Transm, 116*(9), 1111-1162. doi: 10.1007/s00702-009-0240-y

Kaufman, R. J., Scheuner, D., Schroder, M., Shen, X., Lee, K., Liu, C. Y., & Arnold, S. M. (2002). The unfolded protein response in nutrient sensing and differentiation. *Nat Rev Mol Cell Biol, 3*(6), 411-421. doi: 10.1038/nrm829

Kim, W. R., & Sun, W. (2011). Programmed cell death during postnatal development of the rodent nervous system. *Dev Growth Differ, 53*(2), 225-235. doi: 10.1111/j.1440-169X.2010.01226.x

Kirstein-Miles, J., Scior, A., Deuerling, E., & Morimoto, R. I. (2013). The nascent polypeptide-associated complex is a key regulator of proteostasis. *Embo j, 32*(10), 1451-1468. doi: 10.1038/emboj.2013.87

Koplin, A., Preissler, S., Ilina, Y., Koch, M., Scior, A., Erhardt, M., & Deuerling, E. (2010). A dual function for chaperones SSB-RAC and the NAC nascent polypeptide-associated complex on ribosomes. *J Cell Biol, 189*(1), 57-68. doi: 10.1083/jcb.200910074

Lauring, B., Sakai, H., Kreibich, G., & Wiedmann, M. (1995). Nascent polypeptide-associated complex protein prevents mistargeting of nascent chains to the endoplasmic reticulum. *Proc Natl Acad Sci U S A, 92*(12), 5411-5415.

Marciniak, S. J., Yun, C. Y., Oyadomari, S., Novoa, I., Zhang, Y., Jungreis, R., . . . Ron, D. (2004). CHOP induces death by promoting protein synthesis and oxidation in the stressed endoplasmic reticulum. *Genes Dev, 18*(24), 3066-3077. doi: 10.1101/gad.1250704

Mymrikov, E. V., Seit-Nebi, A. S., & Gusev, N. B. (2011). Large potentials of small heat shock proteins. *Physiol Rev, 91*(4), 1123-1159. doi: 10.1152/physrev.00023.2010

Nakagawa, T., Zhu, H., Morishima, N., Li, E., Xu, J., Yankner, B. A., & Yuan, J. (2000). Caspase-12 mediates endoplasmic-reticulum-specific apoptosis and cytotoxicity by amyloid-beta. *Nature, 403*(6765), 98-103. doi: 10.1038/47513

Nishikawa, S., Brodsky, J. L., & Nakatsukasa, K. (2005). Roles of molecular chaperones in endoplasmic reticulum (ER) quality control and ER-associated degradation (ERAD). *J Biochem, 137*(5), 551-555. doi: 10.1093/jb/mvi068

Nishitoh, H., Matsuzawa, A., Tobiume, K., Saegusa, K., Takeda, K., Inoue, K., . . . Ichijo, H. (2002). ASK1 is essential for endoplasmic reticulum stress-induced neuronal cell death triggered by expanded polyglutamine repeats. *Genes Dev, 16*(11), 1345-1355. doi: 10.1101/gad.992302

Ozcan, U., Cao, Q., Yilmaz, E., Lee, A. H., Iwakoshi, N. N., Ozdelen, E., . . . Hotamisligil, G. S. (2004). Endoplasmic reticulum stress links obesity, insulin action, and type 2 diabetes. *Science, 306*(5695), 457-461. doi: 10.1126/science.1103160

Raue, U., Oellerer, S., & Rospert, S. (2007). Association of protein biogenesis factors at the yeast ribosomal tunnel exit is affected by the translational status and nascent polypeptide sequence. *J Biol Chem, 282*(11), 7809-7816. doi: 10.1074/jbc.M611436200

Reimold, A. M., Etkin, A., Clauss, I., Perkins, A., Friend, D. S., Zhang, J., . . . Glimcher, L. H. (2000). An essential role in liver development for transcription factor XBP-1. *Genes Dev, 14*(2), 152-157.

Ron, D., & Walter, P. (2007). Signal integration in the endoplasmic reticulum unfolded protein response. *Nat Rev Mol Cell Biol, 8*(7), 519-529. doi: 10.1038/nrm2199

Rosekrans, S. L., Heijmans, J., Buller, N. V., Westerlund, J., Lee, A. S., Muncan, V., & van den Brink, G. R. (2014). ER stress induces epithelial differentiation in the mouse oesophagus. *Gut*. doi: 10.1136/gutjnl-2013-306347

Rospert, S., Dubaquie, Y., & Gautschi, M. (2002). Nascent-polypeptide-associated complex. *Cell Mol Life Sci, 59*(10), 1632-1639.

Scheuner, D., Song, B., McEwen, E., Liu, C., Laybutt, R., Gillespie, P., . . . Kaufman, R. J. (2001). Translational control is required for the unfolded protein response and in vivo glucose homeostasis. *Mol Cell, 7*(6), 1165-1176.

Shaner, L., Wegele, H., Buchner, J., & Morano, K. A. (2005). The yeast Hsp110 Sse1 functionally interacts with the Hsp70 chaperones Ssa and Ssb. *J Biol Chem, 280*(50), 41262-41269. doi: 10.1074/jbc.M503614200

Shen, X., Ellis, R. E., Sakaki, K., & Kaufman, R. J. (2005). Genetic interactions due to constitutive and inducible gene regulation mediated by the unfolded protein response in C. elegans. *PLoS Genet, 1*(3), e37. doi: 10.1371/journal.pgen.0010037

Sidrauski, C., & Walter, P. (1997). The transmembrane kinase Ire1p is a site-specific endonuclease that initiates mRNA splicing in the unfolded protein response. *Cell, 90*(6), 1031-1039.

Sun, Y., & MacRae, T. H. (2005). Small heat shock proteins: molecular structure and chaperone function. *Cell Mol Life Sci, 62*(21), 2460-2476. doi: 10.1007/s00018-005-5190-4

Vabulas, R. M., Raychaudhuri, S., Hayer-Hartl, M., & Hartl, F. U. (2010). Protein folding in the cytoplasm and the heat shock response. *Cold Spring Harb Perspect Biol, 2*(12), a004390. doi: 10.1101/cshperspect.a004390

Waters, E. R., Lee, G. J., & Vierling, E. (1996). Evolution, structure and function of the small heat shock proteins in plants. *J Exp Bot, 47*(3), 325-338. doi: 10.1093/jxb/47.3.325

Ye, J., Rawson, R. B., Komuro, R., Chen, X., Dave, U. P., Prywes, R., . . . Goldstein, J. L. (2000). ER stress induces cleavage of membrane-bound ATF6 by the same proteases that process SREBPs. *Mol Cell, 6*(6), 1355-1364.

Yoneda, T., Imaizumi, K., Oono, K., Yui, D., Gomi, F., Katayama, T., & Tohyama, M. (2001). Activation of caspase-12, an endoplastic reticulum (ER) resident caspase, through tumor necrosis factor receptor-associated factor 2-dependent mechanism in response to the ER stress. *J Biol Chem, 276*(17), 13935-13940. doi: 10.1074/jbc.M010677200

Yoshida, H., Matsui, T., Hosokawa, N., Kaufman, R. J., Nagata, K., & Mori, K. (2003). A time-dependent phase shift in the mammalian unfolded protein response. *Dev Cell, 4*(2), 265-271.

Yoshida, H., Matsui, T., Yamamoto, A., Okada, T., & Mori, K. (2001). XBP1 mRNA is induced by ATF6 and spliced by IRE1 in response to ER stress to produce a highly active transcription factor. *Cell, 107*(7), 881-891.

Yoshida, H., Oku, M., Suzuki, M., & Mori, K. (2006). pXBP1(U) encoded in XBP1 pre-mRNA negatively regulates unfolded protein response activator pXBP1(S) in mammalian ER stress response. *J Cell Biol, 172*(4), 565-575. doi: 10.1083/jcb.200508145

Yuan, L., Li, X., Feng, J., Yin, C., Yuan, F., & Wang, X. (2014). IRE1alpha is essential for Xenopus pancreas development. *J Biomed Res, 28*(2), 123-131. doi: 10.7555/jbr.28.20130076

Zhang, K., Wong, H. N., Song, B., Miller, C. N., Scheuner, D., & Kaufman, R. J. (2005). The unfolded protein response sensor IRE1alpha is required at 2 distinct steps in B cell lymphopoiesis. *J Clin Invest, 115*(2), 268-281. doi: 10.1172/jci21848

Zhang, Y., Berndt, U., Golz, H., Tais, A., Oellerer, S., Wolfle, T., . . . Rospert, S. (2012). NAC functions as a modulator of SRP during the early steps of protein targeting to the endoplasmic reticulum. *Mol Biol Cell, 23*(16), 3027-3040. doi: 10.1091/mbc.E12-02-0112